Journal of Hazardous Materials 514 (2026) 142572

Contents lists available at ScienceDirect

Journal of Hazardous Materials

journal homepage: www.elsevier.com/locate/jhazmat

Combining equilibrium and dynamical models to describe two-component adsorption in a fixed bed

A. Valverde [a], T.G. Myers [b], A. Cabrera-Codony [c], H.M. Thompson [d], G. Moncusí-Prieto [c], M. Calvo-Schwarzwalder [e,b,f,*]

[a] Department of Chemical Engineering, Universitat Politècnica de Catalunya, Escola Superior d'Enginyeries Industrial, Aeroespacial i Audiovisual de Terrassa, 08222 Terrassa, Spain
[b] Centre de Recerca Matemàtica, Campus de Bellaterra, Edifici C, 08193 Bellaterra, Barcelona, Spain
[c] LEQUIA, Institute of the Environment, Universitat de Girona, 17003 Girona, Catalonia, Spain
[d] School of Mechanical Engineering, University of Leeds, Leeds, United Kingdom
[e] Department of Mathematics, Universitat Politècnica de Catalunya, Escola d'Enginyeria de Telecomunicació i Aeroespacial de Castelldefels, 08860 Castelldefels, Spain
[f] Institut de Matemàtiques-BarcelonaTech, Universitat Politècnica de Catalunya, Facultat de Matemàtiques i Estadistica, 08860 Barcelona, Spain

HIGHLIGHTS

- We present a predictive model for two-component adsorption using isotherm-derived inputs.
- Roll-up and displacement are captured via equilibrium-based dimensionless parameters.
- Binary breakthrough curves accurately predicted with only one fitted kinetic parameter.
- Model validated against seven two-component adsorption tests with high accuracy
- Isotherm prediction outperforms travelling-wave approximation for half-times

GRAPHICAL ABSTRACT

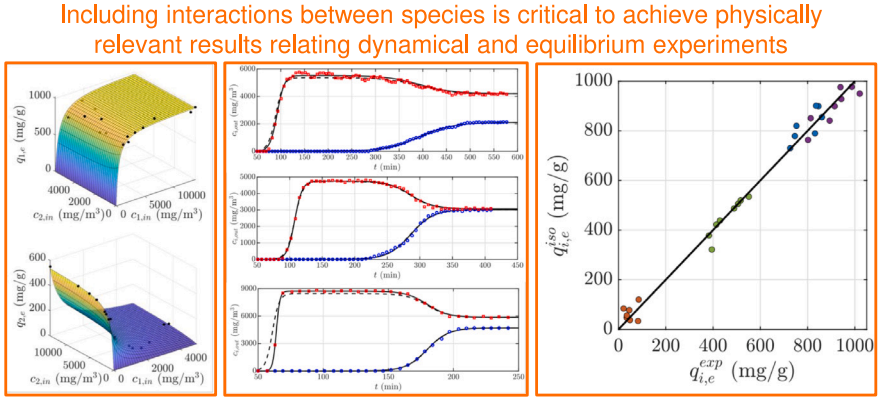

ARTICLE INFO

Dataset link: https://github.com/marccalvoschwarzwalder/TwoComponentIsothermData

Keywords:
Competitive adsorption
Fixed-bed column
Roll-up effect
Multicomponent adsorption
Isotherm fitting

ABSTRACT

We introduce a novel approach for predicting fixed-bed adsorption involving two competing contaminants. The method leads to simple analytical expressions for the concentrations and amount adsorbed throughout the column during an experiment. It primarily relies on equilibrium (isotherm) data, with just a single parameter fitted to breakthrough data. The advantage of employing the isotherm is that the coefficients are obtained using a range and combination of concentrations ensuring a wide range of validity.

The isotherm analysis provides key information such as shifts in breakthrough time due to competition, the magnitude of the roll-up effect and relations between adsorption and displacement rates. From the breakthrough data we are able to determine the coefficient describing the rate at which the dominant species replaces the other species and from this all other coefficients may be calculated. Although the dynamic model neglects desorption it is accounted for through the isotherm analysis.

* Corresponding author.
E-mail address: marc.calvo.schwarzwalder@upc.edu (M. Calvo-Schwarzwalder).

https://doi.org/10.1016/j.jhazmat.2026.142572
Received 12 September 2025; Received in revised form 15 May 2026; Accepted 30 May 2026
Available online 5 June 2026

The method is validated against novel and literature-based competitive column experiments, where the isotherm-based predictions reproduce full curves with $R^2 > 0.95$ and a low relative error. Compared to a previous travelling wave approximation, on which this work is based, the present approach yields similar accuracy with the added advantage of providing physically interpretable parameters and allowing predictions of half-times and roll-up height over a wider range of validity. This may then be used to reduce experimental effort while maintaining strong predictive performance.

1. Introduction

Adsorption is widely applied in gas and water treatment, air pollution control and industrial separation processes. It is based on the ability of solid materials to retain molecules on their surface through physical (physisorption) or chemical (chemisorption) interactions [1]. The efficiency of adsorption depends on factors such as surface area, pore structure, and the nature of the adsorbate-adsorbent interactions [2,3].

Physisorption occurs through weak van der Waals forces, including dispersion forces, dipole–dipole interactions, and hydrogen bonding, making it a reversible process [4,5]. Adsorbed molecules can desorb when external conditions such as temperature or concentration change [6]. This mechanism dominates in porous materials with high surface area, such as activated carbon, zeolites, and metal–organic frameworks (MOFs), which are widely used due to their tuneable adsorption properties [7]. The adsorption capacity in such systems may be described by equilibrium isotherms, such as Langmuir and Freundlich models, which quantify how adsorbates distribute between the solid phase and the bulk phase under equilibrium conditions [8,9]. Chemisorption, in contrast, involves the formation of strong chemical bonds between the adsorbate and the surface, resulting in higher selectivity and often irreversibility. Unlike physisorption, which depends largely on pore structure and available surface area, chemisorption is controlled by the reactivity of surface functional groups. This type of adsorption is critical in heterogeneous catalysis and selective gas separation, such as CO_2 capture using amine-functionalised adsorbent [10–12].

In industrial applications, single-component adsorption is rare. Most systems involve multiple contaminants interacting with the same adsorbent, leading to competitive adsorption, where species compete for available sites, altering adsorption capacities, breakthrough times, and overall removal efficiency [13–16]. Unlike single-component systems, where adsorption follows well-defined equilibrium isotherms, competitive adsorption introduces complex interactions that depend on molecular properties and system conditions [17,18]. The affinity of each adsorbate for the surface is influenced by molecular size and shape, as larger molecules may experience steric hindrance limiting their access to smaller pores [19]. Polarity and functional groups also play a role, with more polar adsorbates favouring polar surfaces, while non-polar molecules interact more effectively with hydrophobic materials. Additionally, adsorption strength is dictated by binding energy, with species exhibiting stronger interaction forces more likely to displace weaker adsorbates [20].

When a high-affinity adsorbate enters a system, it can partially or completely replace a previously adsorbed weaker species, a process known as adsorbate displacement. This occurs when the stronger species preferentially occupies adsorption sites, forcing the weaker adsorbate to return to the effluent stream. As a result, the weaker species experiences an earlier breakthrough and higher effluent concentrations than in a single-component system. The extent of displacement depends on the relative affinities, concentrations, and adsorption kinetics of the competing species, directly influencing the efficiency and stability of adsorption-based separation processes [21].

In some cases, displacement occurs gradually, and the weaker adsorbate desorbs in a controlled manner without exceeding its inlet concentration. However, when a significant amount of the weaker compound is suddenly displaced from the surface, desorption can be abrupt. This results in a temporary overshoot in the effluent concentration, known as the roll-up effect, where the displaced species locally exceeds its inlet level before stabilising. Understanding these competitive adsorption effects are critical for optimising adsorption-based separation systems, as they influence removal efficiency and operational stability in applications such as gas purification, water treatment, and air pollution control [22].

Extensive research has focused on modelling interactions between multiple contaminants and their impact on adsorptive capacity, using approaches like multi-component Langmuir isotherms [23,24], IAST [25,26], and machine learning models [27,28]. These models primarily address equilibrium behaviour and often overlook the dynamics of breakthrough adsorption. Machine learning methods, while powerful, tend to lack physical interpretability and are limited to their training conditions.

To model multi-component adsorption columns, most studies solve coupled PDEs that include mass conservation and a sink term based on the Linear Driving Force (LDF) model. The equilibrium adsorbed fraction is typically defined by time-dependent multi-component isotherms such as Langmuir [29–36], Freundlich [30,34], Langmuir-Freundlich [37–39], and others [40–46]. Most solutions are numerical, although early studies by Cooney et al. [29] and Miura et al. [30] presented analytical solutions based on the constant pattern (travelling wave) approach. While some studies correctly align dynamic models with multi-component isotherms [37], many use inconsistent methods relying on single-component parameters [31–33,38,40–42] or incorporating single-component isotherms in LDF formulations [47,48]. Additionally, the LDF approach often misrepresents equilibrium, which should correspond to the steady-state of the adsorption kinetics. This inconsistency can lead to unphysical predictions, such as the roll-up effect, despite originating from kinetics that only model competition, not displacement. Another common approach in the literature is to assume local adsorption equilibrium, which leads to incorporating the time derivative of the isotherm into the mass balance. In some cases, this arises from choosing inappropriate length and time scales–scales that should properly balance advection with adsorption rates [49,50]. In others, it results in a model that is effectively governed by intra-particle diffusion, even though adsorption-displacement kinetics should be the controlling mechanism [51–55]. Furthermore, in all such cases, equilibrium isotherms are applied without verifying whether they can adequately describe multicomponent equilibrium data, and whether they can also be reduced to consistently represent single-component experimental data.

In this study, we build upon the mathematical model proposed in our previous work, Calvo-Schwarzwalder et al. [56], where we derived an approximate analytical solution for competitive adsorption in a packed bed column. The model describes the dynamics of adsorption and displacement of binary mixtures, providing closed-form expressions for breakthrough curves. The analytical expressions describe the evolution of the concentration and adsorbent occupancy and so provide a practical and computationally efficient alternative to full numerical simulations, with parameters that have clear physical meaning.

In the original study, the model was tested against experimental breakthrough data for two-contaminant systems, successfully capturing competitive adsorption and roll-up effects. However, key parameters, such as the half-times of each species (defined as the time at which the

Nomenclature

Superscripts

a	Adsorption
d	Desorption
e	Equilibrium value
f	Final value
h	Half-time
i (j)	Component i (j)
in	Inlet value
max	Maximal value
out	Outlet value
r	Replacement

Non-dimensional quantities

δ	Competition parameter
λ	Time-shift parameter
C	Concentration ratio
θ	Adsorbed fraction

Dimensional quantities

c	Concentration (mg/m^3, g/L)
K	Equilibrium constants (L/mg)
k	Dynamic rate (L/g min, 1/min)
L	Column length (mm)
M_{ad}	Adsorbent mass (mg)
Q	Flow rate (mL/min)
q	Adsorbed mass per unit mass of adsorbent (mg/g)
q_m	Adsorption capacity (mg/g)
R	Column radius (mm)
t	Time (min)

Subscripts

exp	Obtained from experimental data
iso	Obtained from isotherm

outlet concentration reaches half of the inlet value), had to be extracted from dynamic data. This limited the model's potential as a predictive tool and reduced it to a simple curve-fitting exercise, losing the original physical meaning of the kinetic coefficients and roll-up height.

In this study we extend the framework developed in [56] by combining it with equilibrium information obtained from adsorption isotherms. It is important to determine whether the analytical breakthrough model is consistent with the underlying adsorption mechanism it relies on. Only then can we be confident that the fitted parameters retain their intended physical meaning. Hence, we first show that competitive multi-component Langmuir isotherm – a common model used in adsorption column studies involving multiple contaminants [49–53] – cannot consistently describe both multi- and single-component isotherm data at the same time, which is not true for the isotherm arising from [56], which accounts for competition and displacement. Additionally, isotherm analysis enables the prediction of certain breakthrough parameters without performing dynamic experiments. Thus, the main objective is to predict key breakthrough features — such as breakthrough half-times, the roll-up height and the ratio of adsorption to replacement coefficients — by using the parameters obtained from fitting the isotherm to equilibrium data. This way, we demonstrate that the number of parameters directly fitted to breakthrough data can be reduced to a single kinetic constant and still capture the breakthrough curves. By bridging the gap between equilibrium isotherms and dynamic kinetic modelling, this work provides a computationally efficient tool for predicting multi-component adsorption performance in gas purification, air treatment, and water reuse applications.

2. Experimental investigation

Two types of experimental data sources are considered: literature-based data and original experimental work. The former is taken from Vuong et al. [36], specifically their study on the dynamic adsorption of heptane–cyclohexane binary mixtures. The adsorption of these volatile organic compounds (VOCs) is important not only for obtaining high-purity n-heptane in the petrochemical industry [57], but also because of their presence in urban and industrial areas as environmental pollutants with adverse effects on human health and contributions to global warming [58,59].

Vuong et al. [36] conducted both single-component and binary adsorption experiments using a gaseous stream with nitrogen as carrier fluid at a superficial velocity of 17 cm/s at 25 °C. The experiments were carried out in a stainless steel column 10 cm (8 cm of bed) in height and 1 cm in internal diameter, packed with $M_{ad} = 3$ g of activated carbon (1.24 mm average particle diameter and a bulk density of 472 kg/m^3). Atmospheric pressure is assumed (approximately 1.02 bar). Table SM.7 provides a summary of the operating conditions and physical parameters of the fixed-bed adsorption experiments. The concentration range studied is approximately 3150 to 17 000 mg/m^3 (505 to 4111 ppmv). Although the authors report nominal inlet concentrations of 500, 1000, 2000, and 4000 ppmv, the outlet concentrations at exhaustion suggest that these values are not exact. Therefore, the actual inlet concentration was estimated as the average of the final breakthrough points, where the concentration becomes nearly constant. The average deviation is about 1% for single-component experiments and 6% for multicomponent experiments.

In addition to the datasets used from existing literature, original dynamic adsorption tests were conducted for both single-component and competitive adsorption systems using siloxanes D4 and L2. These compounds are among the most prevalent volatile methylsiloxanes found in biogas and are known to cause severe damage to combustion engines due to silica deposition during combustion. They also compete for adsorption sites in activated carbon filters, which are widely used for biogas purification. Their co-occurrence and similar physicochemical properties make it essential to understand their competitive behaviour in fixed-bed systems [60,61].

The experimental setup involved a glass fixed-bed column with an internal radius of $R = 5$ mm and height of $L = 9$ mm packed with $M_{ad} = 250$ mg of a commercial sample of activated carbon, with particle sizes ranging from 0.212 to 0.425 mm. The activated carbon used in this study was extensively characterised in our previous work (Cabrera-Codony et al. [60], material PhAC-1), where a BET surface area of 1737 m^2 g^{-1}, a total pore volume of 0.91 cm^3 g^{-1}, and a micropore volume of 0.58 cm^3 g^{-1} were reported. The full textural and surface chemistry characterisation, including N_2 and CO_2 adsorption isotherms, pore size distribution (determined by 2D-NLDFT-HS, which is more appropriate for the micro-/mesoporous structure of these carbons than the classical BJH model) and TGA-MS results, is provided in the Supplementary Material (Figures SM.1, SM.2, SM.3 and SM.4).

The test gas was generated by infusing a liquid mixture of the target compounds by a syringe pump (Harvard Apparatus) to a nitrogen stream (99.999%, Abelló Linde) which was regulated by a mass flow controller (Alicat Scientific) to obtain a flow rate $Q = 250$ mL/min. The resulting stream was mixed in four static mixers followed by a 1 L mixing chamber to obtain a test gas with a range of concentrations between 700 and 14 000 mg/m^3. The experiments were carried out at room temperature (23 ± 2 °C). The concentration of each compound at the outlet was continuously measured via a gas sampling valve in a gas chromatograph equipped with a flame ionisation detector (GC-FID, 7589B Agilent Technologies) and a HP-5ms Ultra Inert capillary

column. Each experiment was performed three times, with a variability under 10%. Table SM.1 provides a summary of the operating conditions and physical parameters of the fixed-bed adsorption experiments. The experimental data has been made available online.[1]

Breakthrough curves for each component i were plotted as outlet concentration $c_{i,out}$ (mg/m^3) versus time t (min). The experiment was carried out until the exhaustion time t_f (min), defined as the time when the outlet concentration matches the inlet concentration. The adsorbed amount at equilibrium of each component, $q_{i,e}$, that is, the final adsorbed mass per mass of adsorbent (mg/g) was calculated according to

$$q_{i,e} = \frac{Q}{M_{ad}} \int_0^{\infty} \left(c_{i,in} - c_{i,out}(t)\right)\, dt \approx \frac{Q}{M_{ad}} \int_0^{t_f} \left(c_{i,in} - c_{i,out}(t)\right)\, dt\,, \qquad (1)$$

where $c_{i,in}$ (mg/m^3) is the inlet concentration of component i. Since experimental data is discrete, the integral in Eq. (1) is computed using a trapezoidal rule for $t \in [0, t_f]$.

For consistency and improved accuracy, the equilibrium adsorbed amounts reported by Vuong et al. [36] were calculated for both single-component and multicomponent experiments using Eq. (1), even though the authors provide isotherm data. The calculated values show good agreement with those reported in the original study. For single-component data and for heptane in binary mixtures, the average deviation is about 9%, with a maximum difference of 15%, likely related to the inlet concentration correction and the fact that the amount of adsorbent is reported as approximate. However, some cyclohexane values in the binary experiments show significantly larger discrepancies (up to 60%), probably due to increased experimental noise associated with the roll-up effect.

3. Mathematical modelling

This section presents the analytical framework used to describe and predict competitive adsorption in fixed-bed columns. The model is based on the closed-form breakthrough solution developed by Calvo-Schwarzwalder, Myers, Cabrera-Codony and Valverde (CMCV model) [56], as an extension of the single-contaminant adsorption model, developed by Myers et al. [62], which accounts for competitive adsorption, including displacement effects such as roll-up.

In this study, the model is adapted as a predictive tool by estimating all required parameters from equilibrium adsorption isotherms, except for a single kinetic constant. This enables accurate breakthrough predictions with minimal calibration, offering a practical alternative to full dynamic curve fitting.

3.1. Breakthrough model

The breakthrough model describes how one compound, typically the one being adsorbed the strongest, propagates through the bed and displaces a weaker compound from the adsorbent surface. This interaction gives rise to asymmetric breakthrough curves and, in some cases, to roll-up, where the displaced species temporarily exceeds its inlet concentration in the effluent.

The expressions for the concentrations that will be used as the core of this work were first derived in [56]. In that work, we proposed a dynamic model consisting of one mass transfer and one kinetic equation for each component. After making several assumptions — the most important being that desorption is negligible and that the dominant mechanisms are the adsorption of each species and the displacement of the second species by the first — we were able to derive approximate analytical expressions to describe both the fluid-phase concentrations $c_i(x,t)$ and the adsorbed fractions $\theta_i(x,t)$. The solution is based on identifying travelling wave behaviour in two interacting zones of the bed. The concentrations along the column are given by:

$$c_1(x,t) = \frac{c_{1,in}}{1 + f_1(x,t)}\,, \qquad c_2(x,t) = \frac{(1+\delta)c_{2,in}}{1 + \lambda f_2(x,t)} - \frac{\delta c_{2,in}}{1 + f_1(x,t)}\,. \qquad (2)$$

The adsorbed fractions are

$$\theta_1(x,t) = \frac{1}{1 + f_1(x,t)}\,, \qquad \theta_2(x,t) = \frac{1}{1 + \lambda f_2(x,t)} - \frac{1}{1 + f_1(x,t)}\,. \qquad (3)$$

The functions $f_i(x,t)$ describe the front propagation for each compound:

$$f_1(x,t) = \exp\left[\frac{M k_{1,r} q_{1,m}}{Q}\left(\frac{x}{L} - 1\right) - k_{1,r} c_{1,in}\left(t - t_{1,h}\right)\right]\,, \qquad (4a)$$

$$f_2(x,t) = \exp\left[\frac{M k_{2,a} q_{2,m}}{Q}\left(\frac{x}{L} - 1\right) - k_{2,a} c_{2,in}\left(1+\delta\right)\left(t - t_{2,h}\right)\right]\,, \qquad (4b)$$

where $k_{1,r}$ is the replacement rate constant for species 1, $k_{2,a}$ is the adsorption rate constant for species 2, and $q_{i,m}$ and $t_{i,h}$ are the maximum adsorption capacity and the half-time for each species i. The latter represents the time at which its outlet concentration reaches half of its the inlet value.

The model introduces two key dimensionless numbers: the competition parameter δ and the time-shift parameter λ. The first one quantifies how strongly the dominant species displaces the weaker one,

$$\delta = \frac{q_{2,m}/q_{1,m}}{c_{2,in}/c_{1,in}}\,. \qquad (5)$$

The time-shift parameter λ adjusts the breakthrough delay of the second species,

$$\lambda = 1 + 2\delta \frac{\exp\left(k_{1,r} c_{1,in}\left(t_{1,h} - t_{2,h}\right)\right) - 1}{1 + 2\delta + \exp\left(k_{1,r} c_{1,in}\left(t_{1,h} - t_{2,h}\right)\right)}\,. \qquad (6)$$

The breakthrough curves are obtained by evaluating Eq. (2) at the column outlet, $c_{i,out}(t) = c_i(L,t)$. The resulting time-dependent breakthrough profiles are

$$c_{1,out}(t) = \frac{c_{1,in}}{1 + \exp\left(-k_{1,r} c_{1,in}\left(t - t_{1,h}\right)\right)}\,, \qquad (7a)$$

$$c_{2,out}(t) = \frac{(1+\delta)c_{2,in}}{1 + \lambda \exp\left(-k_{2,a} c_{2,in}(1+\delta)\left(t - t_{2,h}\right)\right)} - \frac{\delta c_{2,in}}{1 + \exp\left(-k_{1,r} c_{1,in}\left(t - t_{1,h}\right)\right)}\,. \qquad (7b)$$

These breakthrough expressions, which are derived in [56] serve as the basis for our study. Here, rather than fitting each breakthrough curve individually, we develop a predictive framework in which all model parameters except $k_{1,r}$ are determined from equilibrium isotherm data. In the next section, we describe the equilibrium adsorption isotherms used to work with the isotherm data.

3.2. Adsorption isotherms

Adsorption isotherms describe the equilibrium relation between the concentration of a compound in the fluid phase and the amount adsorbed on the solid phase.

For a two-component system, equilibrium is reached when concentrations of both species are at their inlet value across the entire column, i.e., when $c_i \equiv c_{i,in}$. The isotherm equations relate these inlet concentrations to the corresponding adsorbed amounts $q_{i,e}$. Following the formulation by [56], the adsorption equilibrium is given by

$$q_{i,e} = \frac{q_{i,m} g_{i,e}}{1 + K_{12} c_{1,in} + K_{21} c_{2,in} + g_{1,e} + g_{2,e}}\,, \qquad (8)$$

where

$$g_{1,e} = K_1 c_{1,in}\left(1 + K_{12} c_{1,in}\right) + K_{11} K_2 c_{1,in} c_{2,in}\,, \qquad (9a)$$

$$g_{2,e} = K_2 c_{2,in}\left(1 + K_{21} c_{2,in}\right) + K_{22} K_1 c_{1,in} c_{2,in}\,. \qquad (9b)$$

[1] https://github.com/marccalvoschwarzwalder/TwoComponentIsothermData.

This formulation captures the combined effects of surface competition, replacement and individual desorption, as originally proposed in the general multi-site Langmuir framework.

The equilibrium constants K_i and K_{ij} describe the adsorption affinities of the components, and are related to the adsorption, desorption and replacement rates through the expressions $K_i = k_{i,a}/k_{i,d}$ and $K_{ij} = k_{i,r}/k_{j,d}$, with the constraint

$$K_{12}K_{21} = K_{11}K_{22}\,. \tag{10}$$

In the absence of replacement effects ($k_{i,r} = 0$, hence $K_{ij} = 0$), the system simplifies to the standard two-component Langmuir isotherm [23, 63],

$$q_{i,e} = \frac{q_{i,m}K_i c_{i,in}}{1 + K_1 c_{1,in} + K_2 c_{2,in}}\,. \tag{11}$$

For a single-component system, where $c_{2,in} = q_{2,e} = 0$, this further reduces to the Langmuir isotherm [64],

$$q_e = \frac{q_m K c_{in}}{1 + K c_{in}}\,, \tag{12}$$

where K is the single-component equilibrium constant.

It is important to note that, although individual desorption mechanisms are explicitly included in the equilibrium formulation, they are neglected in the breakthrough model. Desorption can typically be neglected when the inlet concentration corresponds to a high adsorbed fraction on the isotherm—that is, when it is far enough from the origin. In this case, desorption would only affect the region of the column where concentrations are low. However, in that region, the adsorbed fraction is already close to zero, so the overall impact remains negligible. This condition can be identified for each contaminant by the ratio $1/(K_i c_{i,in}) \ll 1$ [56], which usually holds when the adsorbent has a strong affinity for the contaminant (i.e., high adsorption even at relatively low concentrations). Nevertheless, the influence of desorption is still indirectly captured through the equilibrium constants K_i and K_{ij}, which reflect desorption behaviour under equilibrium conditions.

It should be noted that the values for K_{ij} are determined as lumped equilibrium constants from multi-component isotherm fitting. The decomposition $K_{ij} = k_{i,r}/k_{j,d}$ reflects the underlying kinetic mechanism but does not require independent measurement of each individual rate. Once the single kinetic constant $k_{1,r}$ is obtained from breakthrough fitting, all other kinetic rates can be derived from the definition of the equilibrium constants.

3.3. Parameter estimation

The breakthrough model requires several input parameters describing adsorption capacity, affinity, and kinetics. In this study, most of these parameters are extracted from the adsorption isotherms, enabling a predictive model with minimal reliance on breakthrough curve fitting.

3.3.1. Equilibrium and rate constants

The equilibrium constants K_i and K_i describe the adsorption affinities of the components. The single-component constants K_i are obtained by fitting experimental equilibrium data to the Langmuir isotherm model, while competitive adsorption tests are used to refine the multi-component parameters K_{ij}.

Although desorption appears in the definitions of both K_i and K_{ij}, it is not explicitly included in the analytical breakthrough model. Instead, we assume that, under dynamic conditions, displacement by a stronger competitor dominates the desorption process. As a result, desorption effects are captured indirectly through the fitted equilibrium parameters, and the breakthrough predictions rely only on adsorption and replacement kinetics.

Since adsorption, desorption, and replacement rates are assumed to be concentration-independent [56], the parameters K_i and K_{ij} remain constant across different inlet concentrations. This ensures that the equilibrium constants determined from single-component adsorption tests can be used to predict multi-component behaviour.

Kinetic parameters describe the dynamics of surface occupation. The replacement rate constant $k_{1,r}$ quantifies how quickly the dominant compound displaces a weaker one from the surface, and is obtained by fitting the breakthrough curve of the dominant species.

In contrast, the adsorption rate constant for the second species, $k_{2,a}$, is not fitted but computed from equilibrium constants using the relation:

$$k_{2,a} = \frac{K_2 k_{1,r}}{K_{12}}\,. \tag{13}$$

This approach reduces the number of free parameters in the model to a single kinetic constant, $k_{1,r}$, while maintaining predictive accuracy, minimising the need for dynamic curve fitting.

3.3.2. Competition parameter δ

The parameter δ quantifies the roll-up effect, where a weaker adsorbate is displaced by a stronger one, causing a temporary peak in its breakthrough curve that exceeds its inlet value. This is a characteristic feature of competitive adsorption in fixed-bed system. The model predicts the theoretical maximum concentration as:

$$c_{2,max} =: \max_{t>0}\left[c_{2,out}(t)\right] \approx (1+\delta)c_{2,in}\,. \tag{14}$$

From experimental data, δ^{exp} can be obtained from the breakthrough curve of the displaced compound, using the observed maximum concentration of component 2:

$$\delta^{exp} \approx \frac{c^{exp}_{2,max} - c_{2,in}}{c_{2,in}}\,, \tag{15}$$

where $c^{exp}_{2,max}$ is the peak concentration of $c_{2,out}$ in the breakthrough curve.

Note that this approach requires the roll-up of $c_{2,out}$ to reach a plateau, which occurs when the overlapping travelling waves in Eq. (7b) (the first and second terms corresponding to the right and left far-field waves, respectively) are sufficiently separated in time. This, in turn, implies a sufficiently large delay between the half-times. Otherwise,

$$\delta^{exp} > \frac{c^{exp}_{2,max} - c_{2,in}}{c_{2,in}}\,, \tag{16}$$

and this parameter must then be treated as an additional fitting parameter instead.

In the isotherm-based approach developed in this study, δ does not need to be fitted to dynamic data. Instead, it is predicted directly from equilibrium adsorption isotherms, using only the maximum adsorption capacities and inlet concentrations:

$$\delta^{iso} = \frac{q_{2,m}}{q_{1,m}}\frac{c_{1,in}}{c_{2,in}} = \delta_0 C\,. \tag{17}$$

Here, $\delta_0 = q_{2,m}/q_{1,m}$ is a constant, obtained from the isotherm fitting, and $C = c_{1,in}/c_{2,in}$ represents the inlet concentration ratio, varying across experiments.

This formulation enables the model to capture competition effects quantitatively without additional calibration, supporting the goal of predictive breakthrough modelling based on equilibrium data.

3.3.3. Prediction of half-times

The half-time $t_{i,h}$ is defined as the time at which the outlet concentration of species i reaches half of its inlet value:

$$c_{i,out}\left(t_{i,h}\right) = \frac{c_{i,in}}{2}\,. \tag{18}$$

This characteristic time provides a simple yet informative metric for breakthrough analysis. In dynamic competitive systems, the stronger adsorbate (component 1) typically exhibits a delayed breakthrough, hence $t_{1,h} > t_{2,h}$.

In the travelling wave (TW) approximation proposed by [56], the adsorption front is assumed to propagate at a constant velocity v_i derived from a mass balance. This approximation assumes purely advective transport and neglects desorption and competitive interactions that can accelerate the breakthrough of the weaker compound. The wave propagation velocities are given by:

$$v_1 = \frac{Qc_{1,in}L}{Mq_{1,m}}, \qquad v_2 = \frac{1+\delta}{\delta}v_1, \tag{19}$$

Since the column length is L, the time for the wave centre ($c_i = c_{i,in}/2$) to reach the outlet is approximated as $t_{i,h}^{TW} = L/v_i$, which gives

$$t_{1,h}^{TW} = \frac{Mq_{1,m}}{Qc_{1,in}}, \qquad t_{2,h}^{TW} = \frac{\delta}{1+\delta}t_{1,h}^{TW}. \tag{20}$$

These expressions provide an initial estimate by assuming zero desorption and purely advective transport of the adsorption front.

To refine the estimation, equilibrium adsorption data from isotherms can be incorporated to account for desorption and competitive effects. To this end, we adopt a similar approach to that used by Wilkins et al. [65,66] and Van Assche et al. [67]. Substituting the analytic breakthrough model, Eq. (7), into the equilibrium mass balance Eq. (1) yields the following relations of the adsorbed amounts and the half-time:

$$q_{1,e} = \frac{Q}{Mk_{1,r}}\ln\left[1+\exp\left(k_{1,r}c_{1,in}t_{1,h}\right)\right], \tag{21a}$$

$$\delta_0 q_{1,e} + q_{2,e} = \frac{Q}{Mk_{2,a}}\ln\left[1+\lambda\exp\left((1+\delta)k_{2,a}c_{2,in}t_{2,h}\right)\right]. \tag{21b}$$

Eq. (21a) can be rearranged to determine the half-time of the dominant component:

$$t_{1,h} = \frac{Mq_{1,e}}{Qc_{1,in}} + \frac{\ln\left[1-\exp\left(-\frac{Mk_{1,r}}{Q}q_{1,e}\right)\right]}{k_{1,r}c_{1,in}}. \tag{22}$$

The exponential term in Eq. (22) is proportional to the ratio of the column length to the adsorption length scale. Since the adsorption length is typically much shorter than the column length, the logarithmic term becomes negligible. This leads to the simplified isotherm-based half-time expression of the dominant compound:

$$t_{1,h}^{iso} = \frac{Mq_{1,e}}{Qc_{1,in}}. \tag{23}$$

To obtain the half-time of the second component, we follow a similar approach incorporating the time-shift parameter λ, which accounts for breakthrough time shift due to competition. Assuming $t_{1,h} \gg t_{2,h}$, the expression of λ in Eq. (6) can be simplified to λ^*:

$$\lambda^* \approx 1 + 2\delta\,\frac{\exp\left(k_{1,r}c_{1,in}t_{1,h}^{iso}\right)-1}{1+2\delta+\exp\left(k_{1,r}c_{1,in}t_{1,h}^{iso}\right)}. \tag{24}$$

Substituting this approximation into Eq. (21b) and again neglecting the smaller logarithmic term, we obtain the final isotherm-based estimate for the second component's half-time:

$$t_{2,h}^{iso} = \frac{\delta Mq_{1,m}}{(1+\delta)Qc_{1,in}}\left(\frac{q_{1,e}}{q_{1,m}}+\frac{q_{2,e}}{q_{2,m}}\right) - \frac{\ln(\lambda^*)}{(1+\delta)k_{2,a}c_{2,in}}. \tag{25}$$

3.4. Limitations of the model

The breakthrough model derived in [56] and described by Eqs. (5)–(7) is based on the assumptions outlined in Section 3.1, namely negligible desorption and adsorption/displacement of the second species as the dominant mechanisms. Although desorption effects are partially accounted for through the isotherm parameters, as discussed in the previous sections, the model still depends on the remaining assumptions to allow the formation of a travelling-wave (constant-pattern) solution after an initial transient period.

In well-designed adsorption filters, where column dimensions are chosen to maximise operational lifetime before breakthrough, this transient period is typically short compared with the overall service time, which favours constant-pattern propagation. However, this assumption may no longer hold when adsorbates have similar equilibrium capacities (i.e. similar half-times) but differ significantly in their adsorption kinetics. Consequently, the breakthrough model is restricted to systems with sufficiently distinct half-times, $t_{1,h}$ and $t_{2,h}$. This separation is also required for the derivation leading to Eqs. (23) and (25) to remain valid.

Although situations in which this restriction fails may theoretically occur in industrial columns, they correspond to highly specific operating conditions and are therefore expected to be uncommon.

4. Optimisation routines

To obtain the results that will be discussed in the next section, the equations obtained for the presented model have to be fitted to the experimental data of both isotherm and breakthrough curves. Each of them requires a different optimisation routine.

4.1. Fitting of the single-component isotherm

The values of the isotherm parameters $q_{i,m}$, K_i, K_{ij} must be obtained by taking into account all the two-component experiments. However, we can find a first approximation of the single-component parameters $q_{i,m}$ and K_i by using only single-component experiments. For this we fit Eq. (12) to the available data points (c_{in}, q_e) that can be found in Table SM.2 and Table SM.8 for D4-L2 and heptane-cyclohexane experiments, respectively. This provides a first approximation to the equilibrium constants K_i and the maximal adsorbed amount $q_{i,m}$. For these single contaminant experiments, the experimental conditions are the same as for the two-component ones, summarised in Table SM.1 and Table SM.7. The *fit* function included in the Curve Fitting Toolbox of the software MATLAB® has been used to fit Eq. (12) to the experimental data of each component. The non-linear least squares problem is solved using the Trust-Region algorithm.

As it has been previously pointed out, the value of the parameters obtained by fitting the single-component isotherms are only indicative though, since the multi-component data has not been considered. Thus, K_i and $q_{i,m}$ have to be fitted using the multi-component isotherm equation with all the available data with one and two components at the equilibrium.

4.2. Fitting of the multiple-component isotherm

When dealing with more than one contaminant, fitting requires an optimisation method that works globally, that is, accounting for all the data of all the components simultaneously. In this work, the `GlobalSearch` routine combined with the local optimisation algorithm `fmincon` of the software MATLAB® has been used. The `fmincon` routine uses the interior-point algorithm as default value. The optimisation has been treated as a multi-objective optimisation problem. The two objectives to minimise consist of the multi-component isotherm data of each species. Although the single-component isotherm data is also fitted with equations in Eq. (8), separate objective functions have been defined, since the singularity (either of the inlet concentrations is zero) and different population size of the single-isotherm values can jeopardise the fitting of the multi-component ones. Hence, we account for four objective functions that have to be simultaneously minimised. To avoid potential issues caused by the different magnitudes of the $c_{i,in}$ and $q_{i,e}$ values (see Tables SM.2, SM.3, SM.8, SM.9), we define one objective function for each component and each experiment. This gives a total of 4 objective functions of the form

$$\mathcal{F}_{i,l} = \sum_{j=1}^{N_{i,l}}\left(y_{i,j,l}^{exp} - y_{i,j,l}^{iso}\right)^2, \tag{26}$$

where $\mathcal{F}_{i,l}$ is the objective function of component i ($i = \{1,2\}$) for the single-component ($l = 1$) or multi-component ($l = 2$) data. $N_{i,l}$ is the number of data points of component i for single or multi-component data l, and $y^{exp}_{i,j,l}$ and $y^{iso}_{i,j,l}$ are the experimental and calculated values j, respectively, of adsorbed fraction at equilibrium of component i ($q_{i,e}$) for the single or multi-component data l.

The multi-objective problem then reads

$$\min_X OF = \min_X \left(\sum_{i=1}^{2} \sum_{l=1}^{2} \left(\frac{\mathcal{F}_{i,l} - \mathcal{F}^*_{i,l}}{\mathcal{F}^*_{i,l}} \right)^2 \right)^{\frac{1}{2}}, \quad (27)$$

where $X = \{q_{1,m}, q_{2,m}, K_1, K_2, K_{12}, K_{21}, K_{22}\}$ and $\mathcal{F}^*_{i,l}$ is the individual global minimum of each objective function, i.e. $\mathcal{F}^*_{i,l} = \min_X \mathcal{F}_{i,l}$. Two concepts have been used to define the multi-objective function: the scalarisation of the objective functions with $\mathcal{F}^*_{i,l}$, and the multi-objective function defined as the Euclidean distance between the optimum point and the individual global minima of each objective function. The use of the norm in Eq. (27) as the multi-objective function is a well-known method to define a compromise solution with no a priori nor posteriori articulation of preferences [68,69]. This avoids the need of a decision maker and therefore the possible bias that this would introduce. The scalarisation with $\mathcal{F}^*_{i,l}$ is also common in literature [68,70,71].

5. Results and discussion

Our aim is to validate the use of equilibrium isotherms as the primary input for a predictive breakthrough model, minimising the need for dynamic curve fitting. While previous work [56] introduced the model using direct parameter fitting from breakthrough data, here we demonstrate that except a the replacement constant $k_{1,r}$, all model parameters can be derived from equilibrium isotherms. This includes δ^{iso} (Eq. (17)) and $t^{iso}_{1,h}$ (Eq. (23)), which directly stem from isotherm parameters such as the adsorption capacities $q_{i,m}$ and equilibrium constants K_i and K_{ij}, and λ^* (Eq. (24)), $t^{iso}_{2,h}$ (Eq. (25)) and $k_{2,a}$, which can be calculated using the same isotherm parameters (Eq. (13)) once $k_{1,r}$ is known. This approach allows us to validate the breakthrough model proposed by Calvo-Schwarzwalder et al. [56], consistently linking each parameter to its original physical meaning. It also increases the model's robustness to untested operating conditions, as it enables the prediction of certain breakthrough features, such as δ^{iso} and $t^{iso}_{1,h}$, before conducting dynamic experiments.

5.1. Isotherm fitting

This section presents the isotherm fitting of both single- and two-component systems. The goal is to extract consistent values of K_i, K_{ij} and $q_{i,m}$, which will later be used for breakthrough prediction in subsequent sections.

5.1.1. Single-component systems

Original single-component column adsorption tests were performed for each siloxane D4 and L2, using steam-activated carbon as the adsorbent. Vuong et al. [36] report single-component column adsorption tests for heptane and cyclohexane using steam-activated carbon as the adsorbent. In both cases, the adsorption isotherms were determined by varying the influent concentration and calculating the equilibrium adsorbed amount via numerical integration of the breakthrough data according to Eq. (1). In the case of siloxanes D4 and L2, eight experiments were carried out for each species, with inlet concentrations varying between 700 and 14 000 mg/m^3, see Table SM.2. Vuong et al. [36] report three single-component experiments with heptane and four with cyclohexane with inlet concentrations ranging approximately from 1750 to 17 000 mg/m^3 (505 to 4111 ppmv), see Table SM.8. Note that for single-component experiments, species subscript i are omitted, the inlet concentration and equilibrium adsorbed amount are denoted as c_{in} (mg/m^3) and q_e (mg/g), respectively.

Table 1
Parameters obtained from fitting the single-component isotherm to the D4 and L2 original equilibrium data, and heptane and cyclohexane equilibrium data calculated from single-component breakthrough curves by Vuong *et al.* [36].

Parameter	Units	D4	L2	Heptane	Cyclohexane
q_m	mg/g	1004.7	558.0	281.8	275.7
K	L/mg	3.047	1.891	0.379	0.698
SSE	(mg/g)^2	10031	352.2	413.93	1010.3
R^2	–	0.757	0.984	0.988	0.975

The resulting single adsorption isotherms for heptane, cyclohexane and siloxanes D4 and L2 are shown in Fig. 1, where the Langmuir isotherm model, Eq. (12), was fitted to the experimental data to estimate the equilibrium constants (K) and maximum adsorption capacities (q_m) for each compound. To evaluate the accuracy, goodness-of-fit metrics such as the sum of squared errors (SSE) and the coefficient of determination (R^2) were computed (Table 1).

For the siloxanes D4 and L2, the Langmuir model shows strong agreement for both compounds, particularly for L2 (R^2 = 0.984 and SSE = 352.2 (mg/g)^2), indicating excellent consistency with the experimental data. Although the fit for D4 shows a lower R^2 value of 0.757, likely related to the higher scatter in the experimental data as discussed above, the SSE value remains small compared to the squared minimum q_e value. Importantly, the multi-component isotherm fitting (Section 5.1.2), which incorporates additional equilibrium data, yields consistent parameter estimates, indicating that the single-component variability does not compromise the overall predictive framework. The fit to the equilibrium values calculated from the single-component breakthrough curves reported by Vuong et al. [36] also shows good agreement with the Langmuir model (R^2 above 0.974). As observed for the siloxane isotherms, the SSE values remain small compared to the square of the minimum fitted q_e value (26 354 mg^2/g^2).

The adsorption of VOCs such as heptane and cyclohexane, as well as siloxanes, onto activated carbon is predominantly physical [72,73]. This type of adsorption is typically described by Langmuir kinetics, given its clear physical basis [62,74]. The use of alternative models, such as the Sips isotherm (also known as Langmuir–Freundlich) [75], can be misleading in these cases, as the introduction of empirical exponents without a clear physical meaning may reduce the model to a purely fitting tool. The fitting of single-component equilibrium data for D4, L2, heptane, and cyclohexane using the Sips isotherm is provided in the Supplementary Material (Figure SM.5 and Table SM.13). For siloxanes D4 and L2, the goodness of fit is similar to that obtained with the Langmuir isotherm, as the fitted exponent is close to unity. In contrast, for heptane and cyclohexane, a better fit is achieved, but at the expense of obtaining unphysical parameter values (very large q_m and very small K), likely due to the limited range of experimental data.

5.1.2. Two-component systems

For seven and nine column adsorption tests involving competing compounds D4-L2 and heptane-cyclohexane, respectively, the equilibrium values $q_{i,e}$ for each compound i were calculated through numerical integration of the breakthrough data $c_{i,out}$, as outlined in Eq. (1). The influent concentrations of siloxanes D4 and L2 ranged from 1600 to 6000 mg/m^3, with the concentration ratios (concentration D4/concentration L2) between 0.30 and 1.02 (Table SM.3). In the case of the heptane-cyclohexane mixture, the influent concentrations approximately ranged from 3150 to 17 000 mg/m^3 (894 to 4011 ppmv), with the concentration ratios (concentration heptane/concentration cyclohexane) between 0.29 and 5.25 (Table SM.9).

The isotherms for both components of the same mixture were simultaneously fitted using a multi-objective optimisation procedure that accounts for the interactions between the components through the cross-equilibrium constants K_{ij}, the single-component equilibrium constants K_i, and the maximum capacities $q_{i,m}$. The model used the two-component isotherm function $q_{i,e}(c_{1,in}, c_{2,in})$ defined in Eq. (8), while

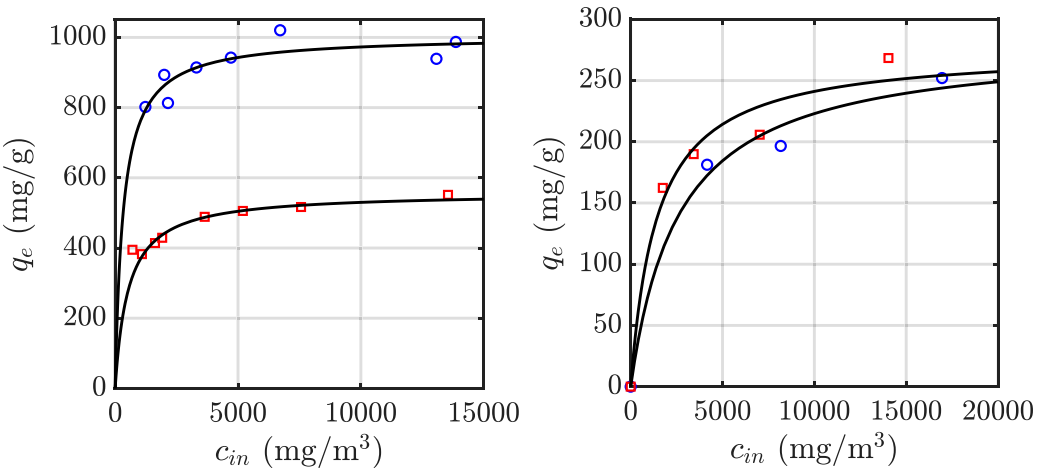

Fig. 1. Fitting of the single-component Langmuir isotherm (Eq. (12)) to experimental equilibrium data at different inlet concentrations. Left panel: Component 1 (D4, blue) and Component 2 (L2, red). Right panel: Component 1 (heptane, blue) and Component 2 (cyclohexane, red).

Eq. (10) was applied to reduce the number of fitting parameters to seven: $q_{1,m}$, $q_{2,m}$, K_1, K_2, K_{12}, K_{21} and K_{22}.

The results of the global optimisation to siloxanes D4-L2 and heptane-cyclohexane binary mixtures equilibrium data are shown in Figs. 2(a) and 3(a), respectively, with the corresponding parameter values summarised in Table 2. A detailed explanation of the optimisation procedure is provided in Section 4.

As expected, the SSE for the two-component systems where higher than for the single-component systems, reflecting the increased complexity of the multi-objective optimisation. However, the optimisation process successfully identified an optimal balance between the two isotherms for both mixtures, with similar SSE_i values for both components in each case. While the global SSE (4.199×10^4 and 7.656×10^3 $(mg/g)^2$ for D4-L2 and heptane-cyclohexane mixtures, respectively) may seem large, they are of the same order as the squared minimum adsorbed amounts measured for each case, confirming the fit's adequacy. The model achieved a strong fit for L2, with an R_2^2 value of 0.977. For D4, the fit was lower ($R_1^2 = 0.752$), likely due to increased noise in the experimental data. Despite this, the overall fit quality of the siloxanes two-component system is excellent, with $R^2 = 0.976$. Furthermore, the balanced SSE values (2.692×10^4 vs. 1.507×10^4 $(mg/g)^2$) confirm that the optimisation did not sacrifice one component for the other. In the case of the heptane–cyclohexane mixture, the model shows very good agreement with the isotherms of both components. The overall fit is comparable to that obtained for the siloxane mixture ($R^2 = 0.952$), while the SSE is lower, partly because the $q_{i,e}^{iso}$ values are smaller.

When comparing the two-component isotherm parameters ($q_{i,m}$ and K_i, Table 2) with those from the single-component isotherm (q_m and K, Table 1), the differences for q_m are small. The maximum adsorption capacities differ by only 0.6% for D4–L2 and 6% for the heptane–cyclohexane system. Larger deviations are observed for the equilibrium constants: K_1 varies by 4% (D4–L2) and 20% (heptane–cyclohexane), while K_2 varies by 18% (D4–L2) and 9% (heptane–cyclohexane). Despite these differences, the agreement with the single-component isotherm data remains very good. When only these data points are considered, the goodness-of-fit indicators ($R^2 = 0.805$ and $R^2 = 0.981$ for D4 and L2, and $R^2 = 0.987$ and $R^2 = 0.973$ for heptane and cyclohexane) are nearly unchanged with respect to those in Table 1. This suggests that the global optimisation of both single- and multicomponent isotherm data provides additional valuable information, leading to more accurate isotherm parameters that consistently describe both systems. This consistency also reinforces the assumptions made in the derivation of the analytical approximations (Eq. (7)) and which are summarised in Section 3.1.

The surface plots generated using the two-component Langmuir isotherm, Eq. (11), are shown in Figs. 2(b) and 3(b). Because Eq. (11) contains no additional parameters besides those obtained from fitting each single-component Langmuir isotherm, Eq. (12), the parameter values listed in Table 1 were used to construct both figures. The large discrepancies between the isotherm surfaces and the experimental data indicate that it is not possible to find a single set of parameters that simultaneously fits both multi- and single-component data.

Table 2
Parameters obtained from fitting the multi-component isotherm (Eq. (8)) to the D4-L2 and heptane-cyclohexane equilibrium adsorption data for both components of each mixture, including single- and two-component systems. K_{11} is determined by $K_{11} = K_{12}K_{21}/K_{22}$.

Parameter	Units	D4	L2	Heptane	Cyclohexane
$q_{i,m}$	mg/g	1004.9	554.8	266.0	264.9
K_i	L/mg	2.571	1.966	0.475	0.642
K_{1i}	L/mg	1.397	1.124	0.276	0.419
K_{2i} ($\times 10^{-9}$)	L/mg	3.113	2.505	7770	11 790
SSE_i ($\times 10^4$)	$(mg/g)^2$	2.692	1.507	0.318	0.447
R_i^2	–	0.752	0.977	0.932	0.948
SSE ($\times 10^4$)	$(mg/g)^2$	4.199		0.765	
R^2	–	0.976		0.952	

The strong agreement between experimental and calculated multicomponent adsorbed fractions using CMCV's isotherm, Eq. (8), is demonstrated by the diagonal trend of the points in Figs. 4(a) and 5(a). In contrast, the large deviation from the diagonal line of the points predicted by the two-component Langmuir isotherm (Eq. (11)) in Figs. 4(b) and 5(b) highlights the significant error and inadequacy of this model. This further shows that the displacement term introduced by Calvo-Schwarzwalder et al. [56] is a key mechanism for accurately modelling these binary adsorption systems.

The same approach was used to assess the agreement between the two-component equilibrium data for the D4–L2 and heptane–cyclohexane mixtures and the two-component Sips isotherm [76]. The results are presented in the Supporting Material (Figures SM.6 and SM.7). For the D4–L2 system, the mismatch between experimental and predicted values is similar to that observed with the two-component Langmuir isotherm, mainly due to the similarity between the single-component Sips and Langmuir models. In the case of the heptane–cyclohexane system, the fit improves for component 1, but at the expense of a poorer description of component 2. Moreover, this improvement is achieved with unphysical equilibrium parameters (very large $q_{i,m}$ and very small K_i). Taken together with the overall poor agreement, these results highlight the limitations of the Sips model for describing these systems.

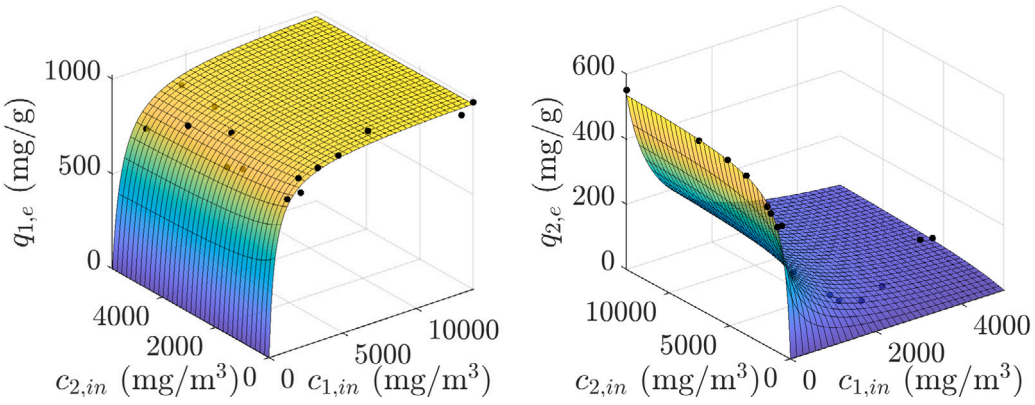

(a) CMCV isotherm

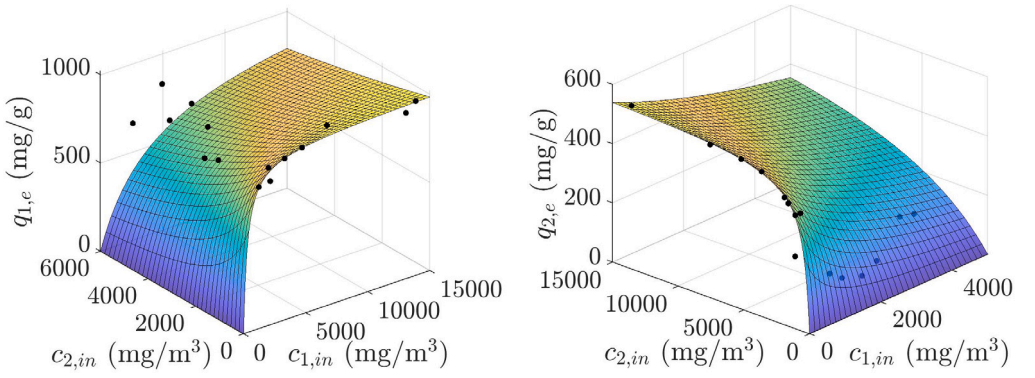

(b) Two-component Langmuir isotherm

Fig. 2. Surface plots showing predicted equilibrium adsorbed amounts as functions of both inlet concentrations of the siloxanes D4 ($i = 1$) and L2 ($i = 2$). Dots indicate experimental measurements. (a) Fitted two-component isotherm by Calvo-Schwarzwalder et al. [56], Eq. (8). (b) Two-component Langmuir isotherm, Eq. (11), using parameters from Table 1.

5.2. Competitive displacement and the prediction of breakthrough shift

In competitive adsorption systems, the breakthrough of the weaker compound can be delayed due to displacement by a stronger adsorbate. This behaviour is captured in the analytical breakthrough model using two dimensionless parameters: the competition parameter δ and the time-shift parameter λ.

The parameter $\delta = q_{2,m}c_{1,in}/(q_{1,m}c_{2,in})$ quantifies how strongly one compound displaces the other from the adsorbent surface, and varies across the tests depending on the influent concentration ratio. It is derived from the parameter $\delta_0 = q_{2,m}/q_{1,m}$ (Eq. (17)), which is directly determined by the results of the isotherm fitting.

The parameter λ is defined in Eq. (6) and appears in the analytical expression for the breakthrough curve of the weaker compound, where it controls the temporal shift of the front compared to a non-competitive system.

To analyse the intensity of the displacement effect, we define the non-dimensional time difference τ:

$$\tau = k_{1,r}\, c_{1,in}(t_{1,h} - t_{2,h})\,. \tag{28}$$

Expressed in terms of this variable, λ becomes

$$\lambda(\tau) = 1 + 2\delta \cdot \frac{e^{\tau} - 1}{1 + 2\delta + e^{\tau}}\,. \tag{29}$$

Fig. 6 illustrates the resulting behaviour. When half-times are similar ($\tau \approx 0$), λ remains close to 1, indicating minimal breakthrough delay. As τ increases, λ increases in a non-linear fashion and approaches a maximum value of $1 + 2\delta$, which corresponds to complete displacement of the weaker compound.

The steepness and location of this transition are influenced by both δ and the replacement rate constant $k_{1,r}$, which together determine how quickly the displacement effect saturates.

In the original formulation, δ was fitted to breakthrough data. To evaluate the predictive capacity of the isotherm-derived parameter δ^{iso}, we compare it to the experimental estimates δ^{exp}. For the siloxane D4–L2 mixture, δ^{exp} values are obtained using Eq. (15) from seven breakthrough tests under different competitive conditions. The same approach was applied to calculate δ^{exp} for six breakthrough tests reported by Vuong et al. [36]. However, the tests performed at higher heptane inlet concentrations (between 14 845 and 16 539 mg/m^3, i.e., 3600 to 4011 ppmv) do not exhibit a plateau at $c^{exp}_{2,max}$. As discussed in Section 3.3.2, this leads to Eq. (16), in which case δ^{exp} is treated as a fitting parameter.

Fig. 7 presents this comparison as function of the influent concentration ratio $C = c_{1,in}/c_{2,in}$. The values of δ^{exp} follow a linear trend with C, and the regression fit yields a slope close to δ_0, supporting the validity of isotherm-based approach.

Relative deviations between δ^{exp} and δ^{iso}, detailed in Tables SM.4 and SM.10, are mainly observed at lower values of δ for the D4–L2 system, and at higher values of δ for the heptane–cyclohexane system. These deviations are related to small discrepancies in the equilibrium constants, which have a stronger impact on the calculated values. It should be noted that the deviation is predominantly positive for the D4–L2 mixture and negative for the heptane–cyclohexane mixture. The consistent agreement across all tests confirms that δ derived from equilibrium data accurately captures the extent of adsorbate displacement in dynamic conditions. It therefore justifies its use as a fixed, predictive input in the breakthrough model.

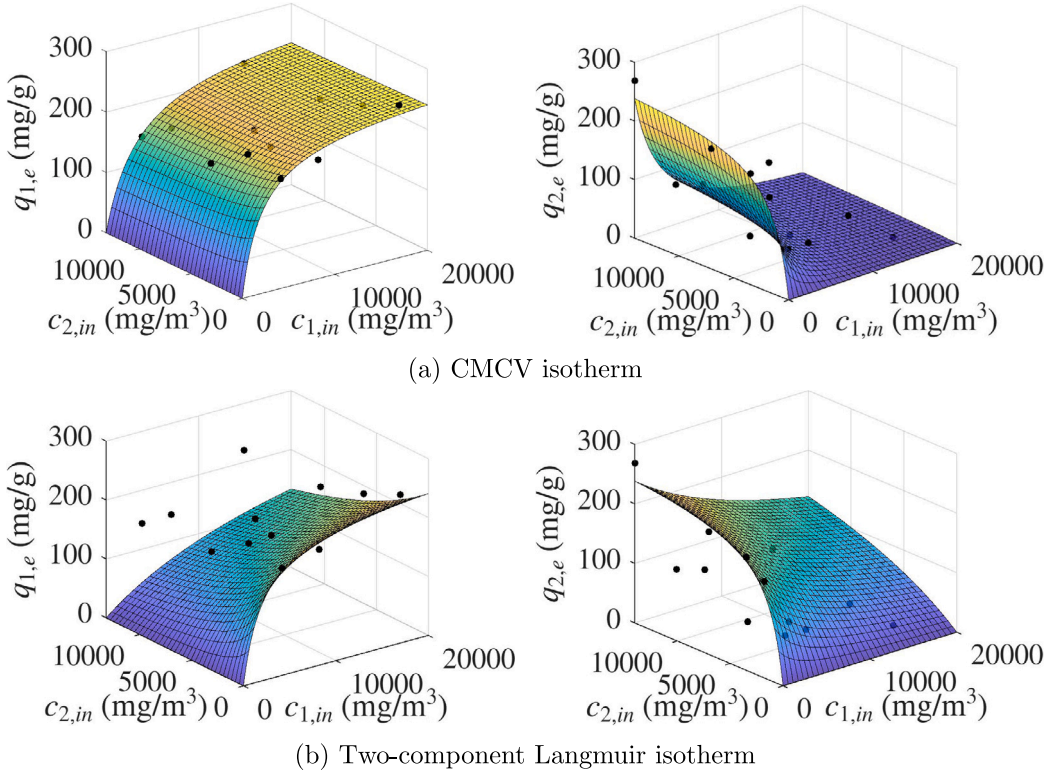

Fig. 3. Surface plots showing predicted equilibrium adsorbed amounts as functions of both inlet concentrations of the VOCs heptane ($i = 1$) and cyclohexane ($i = 2$). Dots indicate experimental measurements. (a) Fitted two-component isotherm by Calvo-Schwarzwalder et al. [56], Eq. (8). (b) Two-component Langmuir isotherm, Eq. (11), using parameters from Table 1.

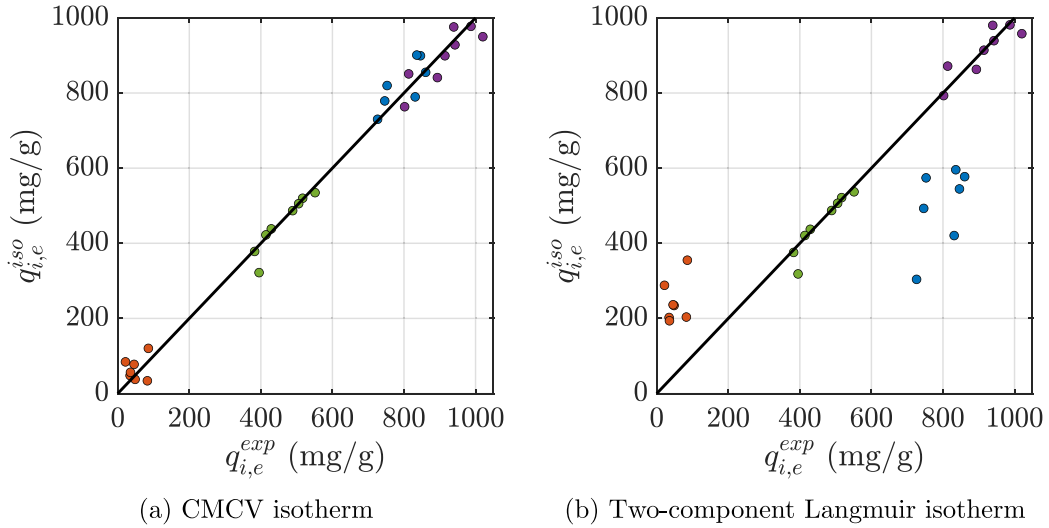

Fig. 4. Comparison of experimental adsorbed fractions ($q_{i,e}^{exp}$) and calculated values ($q_{i,e}^{iso}$) for D4-L2 mixture using (a) the two-component isotherm by Calvo-Schwarzwalder et al. [56], Eq. (8), with parameters from Table 2; (b) the two-component Langmuir isotherm, Eq. (11), with parameters from Table 1. Dots in blue and red for $q_{1,e}$ and $q_{2,e}$ from multi-component experiments. Dots in magenta and green for $q_{1,e}$ and $q_{2,e}$ from single-component experiments.

5.3. Prediction of breakthrough front positions

The analytical model requires the half-times $t_{i,h}$ to define the location of the breakthrough fronts. To assess the accuracy of the isotherm-based predictions, we compare the half-times for both components against experimental breakthrough times from seven two-component adsorption tests with siloxanes D4-L2 mixture and nine with heptane-cyclohexane mixture. Thus, Fig. 8 presents this comparison for both mixtures, including predictions from both the isotherm-based model and the travelling-wave (TW) approximation.

The TW approximation [56] assumes that the adsorption front propagates at a constant velocity, provided in Eq. (19), without considering individual desorption kinetics. By ignoring desorption, the final adsorbed mass, which is equivalent to the maximum in this case, is overestimated. As a result, TW systematically overestimates $t_{2,h}$. This effect is more pronounced for the heptane–cyclohexane mixture, likely due to stronger desorption.

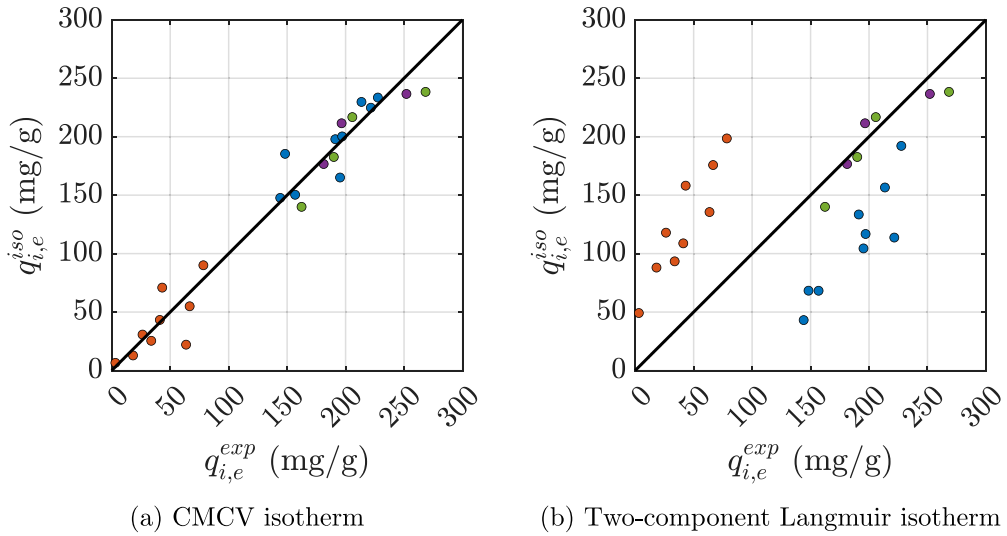

(a) CMCV isotherm (b) Two-component Langmuir isotherm

Fig. 5. Comparison of experimental adsorbed fractions ($q_{i,e}^{exp}$) and calculated values ($q_{i,e}^{iso}$) for heptane-cyclohexane mixture using (a) the two-component isotherm by Calvo-Schwarzwalder et al. [56], Eq. (8), with parameters from Table 2; (b) the two-component Langmuir isotherm, Eq. (11), with parameters from Table 1. Dots in blue and red for $q_{1,e}$ and $q_{2,e}$ from multi-component experiments. Dots in magenta and green for $q_{1,e}$ and $q_{2,e}$ from single-component experiments.

In contrast, the isotherm-based approach proposed here predicts $t_{1,h}$ from the adsorbed amount calculated via Eq. (1) and inlet concentrations. The breakthrough time of the weaker compound, $t_{2,h}$, is then computed using Eq. (25), which incorporates the competition parameter δ, the time-shift parameter λ and the replacement rate constant $k_{1,r}$.

As shown in Fig. 8, the isotherm-based predictions closely match the experimental half-times for both components in both mixtures, with small relative errors across all datasets (see Tables SM.5 and SM.11). The maximum and mean errors obtained with the isotherm-based predictions (6% and 2.8%, respectively) would increase by approximately a factor of 10 for the D4–L2 system and 15 for the heptane–cyclohexane system when using the travelling wave predictions.

5.4. Predicting breakthrough curves from equilibrium data

The final validation step involves comparing experimental breakthrough curves with model predictions to assess the accuracy of the isotherm-based approach. In this framework, the isotherm parameters are used to predict the full breakthrough behaviour of both components of each mixture with minimal fitting, while a fully calibrated, direct-fitting method is used as a reference for comparison (Figs. 9–11).

For the direct fitting, all parameters in the breakthrough expression Eq. (7) are optimised against the experimental data for each curve using the Curve Fitting Toolbox of the software MATLAB®, where the non-linear least-squares problem was solved using the Trust-Region algorithm.

As expected, this yields excellent agreement for both components across all tests. However, it requires full curve-specific calibration and offers limited predictive value beyond the tested conditions.

In contrast, the isotherm-based prediction relies on a single fitter parameter, the replacement rate constant $k_{1,r}$, obtained from the breakthrough curve of the dominant species of each mixture, respectively D4 and heptane, using Eq. (7a). All other model inputs — including adsorption capacities $q_{i,m}$, equilibrium constants K_i, the competition parameter δ, and the breakthrough half-times $t_{i,h}$ — are derived directly from isotherm fitting (Sections 5.1–5.3). The breakthrough curve of the second compound of each mixture, respectively L2 and cyclohexane, is predicted analytically using Eq. (7b) without using its experimental data.

Figs. 9–11 and 12–14 present the isotherm-based predictions for six datasets of the D4–L2 and heptane–cyclohexane competitive adsorption systems, respectively. The remaining datasets (D4–L2 dataset 7 and heptane–cyclohexane datasets 7, 8, and 9) are provided in the Supplementary Material (Figures SM.8 and SM.9). Despite the minimal calibration, the model accurately reproduces the breakthrough profiles of both compounds for both mixtures. The inability to distinguish between solid and dashed lines in some cases, indicates that the isotherm-based predictions and the results from direct optimisation are indistinguishable from one another. Tables 3 and 4 present the quantitative summary of the results for the D4-L2 and heptane-cyclohexane mixtures, respectively. Results from the D4-L2 system show $R^2 > 0.99$ in most cases and only moderately higher SSE values compared to the fully fitted model (see Table SM.6). Although the SSE values obtained for the heptane–cyclohexane mixture are of the same order of magnitude as those for the D4–L2 system, the R^2 values are slightly lower, likely due to higher experimental noise and the presence of some anomalous data points (see, for example, Figs. 13 and 14). Nevertheless, $R^2 > 0.97$ is

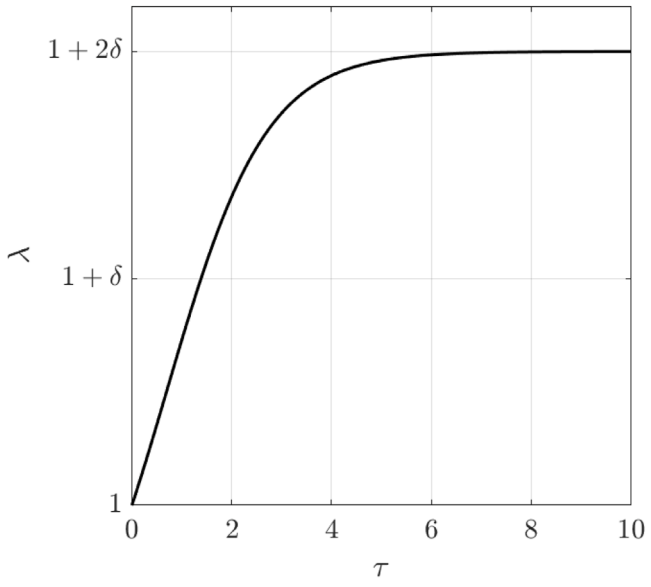

Fig. 6. Qualitative behaviour of the non-dimensional number λ as a function of the difference between the half-times and the displacement rate via $\tau = k_{1,r}c_{1,in}(t_{1,h} - t_{2,h})$.

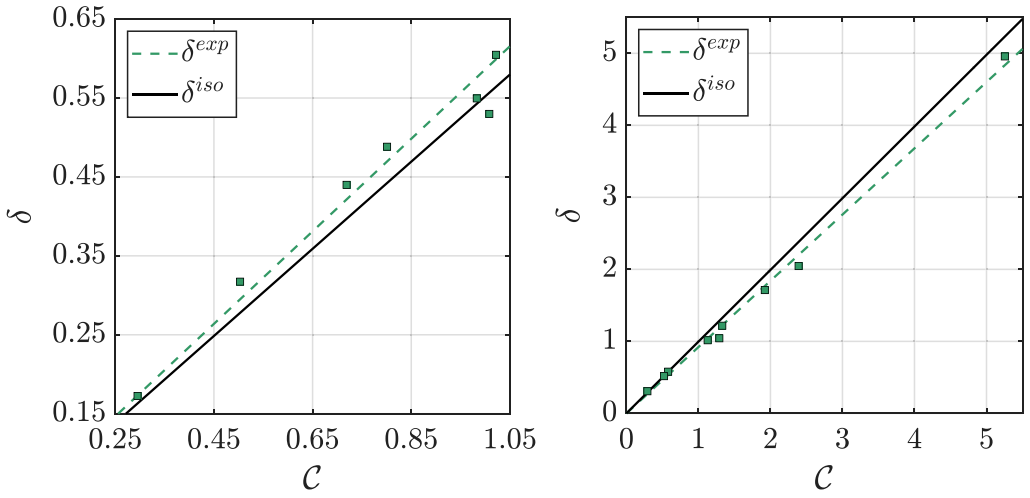

Fig. 7. Comparison of the competition parameter δ determined experimentally (δ^{exp}, squares) and predicted from isotherm fitting (δ^{iso}, solid line) as function of the initial concentration ratio $\mathcal{C} = c_{1,in}/c_{2,in}$. The dashed line represents the linear regression of δ^{exp}. Left panel: siloxanes D4-L2 mixture. Right panel: VOCs heptane-cyclohexane mixture [36].

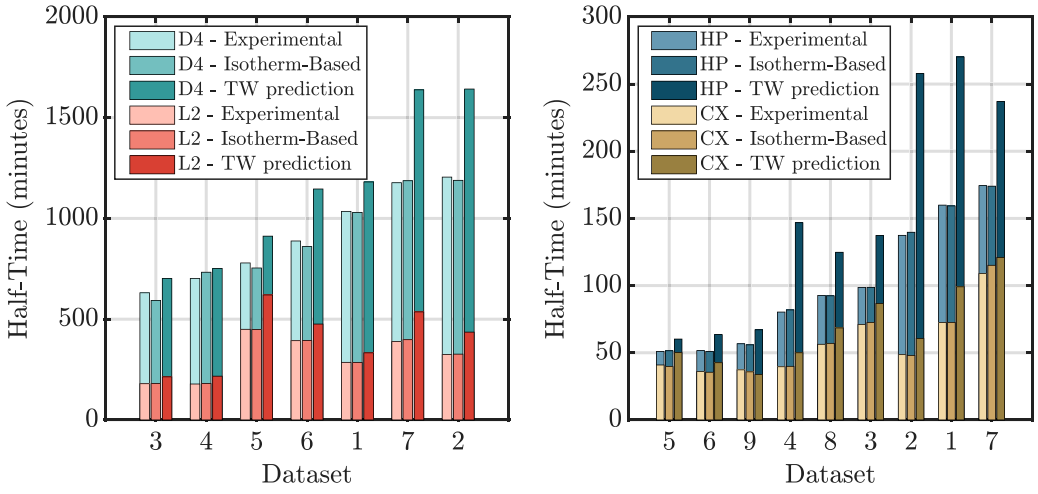

Fig. 8. Comparison of the experimental, isotherm-based predicted, and travelling-wave (TW) -predicted half-times for the two components. Left panel: D4 ($t_{1,h}$) and L2 ($t_{2,h}$). Right panel: heptane (HP, $t_{1,h}$) and cyclohexane (CX, $t_{2,h}$). Datasets are ordered by the breakthrough time of D4 (left panel) and heptane (right panel).

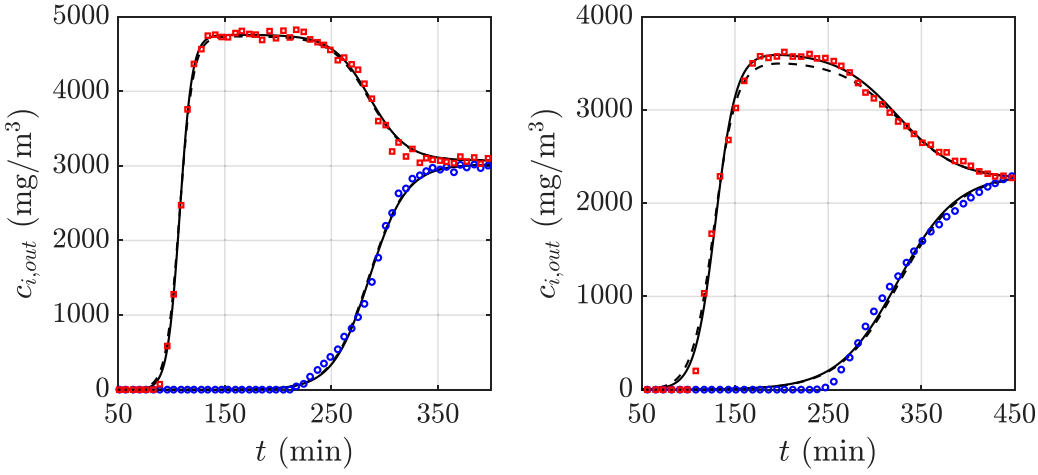

Fig. 9. Comparison between experimental and modelled breakthrough curves for D4 (blue) and L2 (red) across datasets 1 (left panel) and 2 (right panel). Dashed lines represent predictions using equilibrium-derived parameters, while solid lines show results from direct optimisation of Eq. (7) to experimental data.

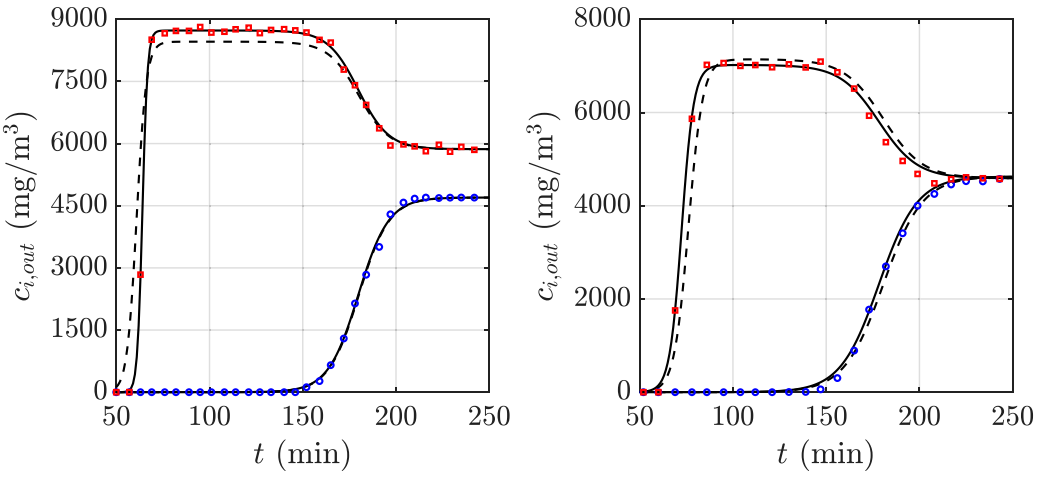

Fig. 10. Comparison between experimental and modelled breakthrough curves for D4 (blue) and L2 (red) across datasets 3 (left panel) and 4 (right panel). Dashed lines represent predictions using equilibrium-derived parameters, while solid lines show results from direct optimisation of Eq. (7) to experimental data.

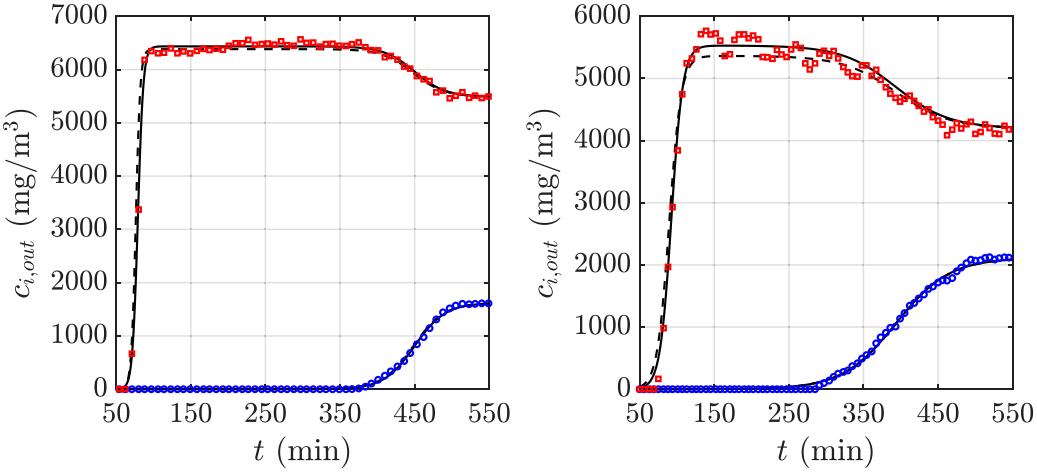

Fig. 11. Comparison between experimental and modelled breakthrough curves for D4 (blue) and L2 (red) across datasets 5 (left panel) and 6 (right panel). Dashed lines represent predictions using equilibrium-derived parameters, while solid lines show results from direct optimisation of Eq. (7) to experimental data.

Table 3
Parameter values obtained from fitting $c_{i,out}/c_{i,in}$, with $c_{i,out}$ defined in Eq. (7), to the breakthrough curve of datasets 1 to 7 of D4-L2 mixture adsorption using the isotherm-based estimation method. Only $k_{1,r}$ is fitted, while the remaining parameters are derived from equilibrium constants.

Dataset	1	2	3	4	5	6	7
$k_{1,r}$ ($\times 10^3$ L/g min)	0.019	0.014	0.026	0.021	0.030	0.013	0.012
$k_{2,a}$ ($\times 10^3$ L/g min)	0.033	0.024	0.046	0.037	0.052	0.023	0.023
δ^{iso} (–)	0.543	0.564	0.442	0.557	0.163	0.278	0.397
$t_{1,h}^{iso}$ (min)	102.7	117.5	64.90	65.00	161.4	141.7	143.3
$t_{2,h}^{iso}$ (min)	370.6	427.9	213.5	264.0	271.4	309.7	427.1
SSE_1 (–)	0.020	0.044	0.005	0.008	0.013	0.026	0.175
SSE_2 (–)	0.038	0.088	0.366	0.174	0.100	0.186	0.131
R_1^2	0.998	0.997	0.999	0.999	0.999	0.998	0.989
R_2^2	0.998	0.996	0.974	0.984	0.991	0.989	0.992

Table 4
Parameter values obtained from fitting $c_{i,out}/c_{i,in}$, with $c_{i,out}$ defined in Eq. (7), to the breakthrough curves of datasets 1 to 9 of heptane-cyclohexane mixture adsorption using the isotherm-based estimation method. Only $k_{1,r}$ is fitted, while the remaining parameters are derived from equilibrium constants.

Dataset	1	2	3	4	5	6	7	8	9
$k_{1,r}$ (L/g min)	0.443	0.449	0.402	0.493	0.324	0.250	0.533	0.360	0.195
$k_{2,a}$ (L/g min)	0.678	0.687	0.615	0.754	0.496	0.382	0.815	0.552	0.299
δ^{iso} (–)	0.578	0.291	1.914	0.520	5.232	2.381	1.285	1.326	1.123
$t_{1,h}^{iso}$ (min)	159.3	139.7	98.72	81.85	51.54	50.95	174.02	92.44	55.90
$t_{2,h}^{iso}$ (min)	72.58	48.00	72.46	39.85	39.68	35.51	115.08	56.97	35.74
SSE_1 (–)	0.021	0.107	0.030	0.055	0.108	0.053	0.020	0.079	0.029
SSE_2 (–)	0.029	0.237	0.865	0.726	2.089	0.585	7.553	1.103	0.418
R_1^2	0.995	0.972	0.991	0.983	0.981	0.986	0.995	0.984	0.990
R_2^2	0.997	0.971	0.964	0.913	0.968	0.973	0.574	0.941	0.961

achieved in most cases, along with only moderately higher SSE values compared to the fully fitted model (see Table SM.12).

Notable deviations occur in D4-L2 mixture datasets 3 and 4, and heptane-cyclohexane mixture datasets 3, 7 and 9, where the predicted shape of the curve of component 2 diverges more clearly from the experimental profile. These cases also correspond to the largest differences in $t_{i,h}$ observed in Figs. 10, 13 and SM.9, suggesting that uncertainties in the isotherm parameters may propagate through $q_{i,e}$ to the predicted breakthrough position and curve shape, as the equilibrium values $q_{i,e}$ are computed by integrating the breakthrough data (Eq. (1)). The reduced number of data points in D4-L2 mixture datasets 3 and 4 may be a possible cause for these deviations. In the case of the heptane–cyclohexane system, errors in the calculation of $q_{i,e}$ are mainly attributed to noise in the experimental data, which strongly affects the numerical integration. The deviations observed in the cyclohexane curve in dataset 9 are directly linked to those in the heptane curve,

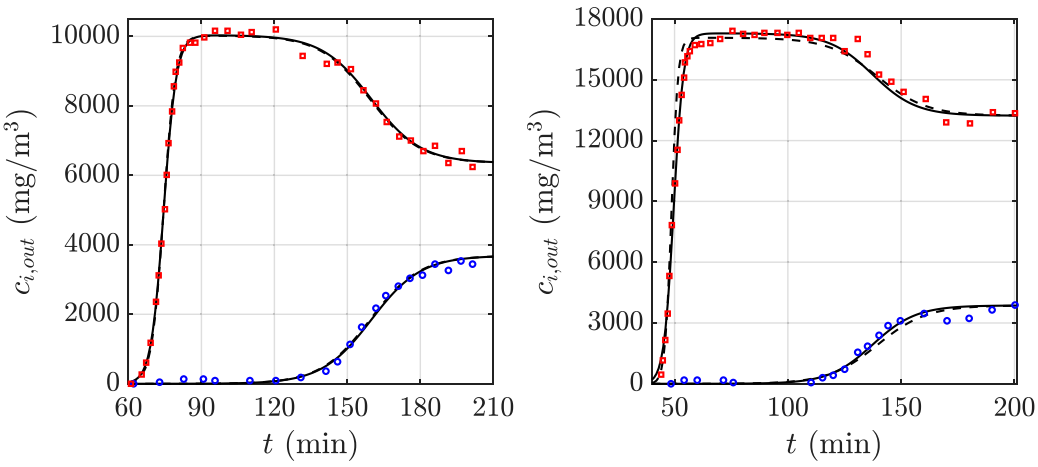

Fig. 12. Comparison between experimental and modelled breakthrough curves for heptane (blue) and cyclohexane (red) across datasets 1 (left panel) and 2 (right panel). Dashed lines represent predictions using equilibrium-derived parameters, while solid lines show results from direct optimisation of Eq. (7) to experimental data.

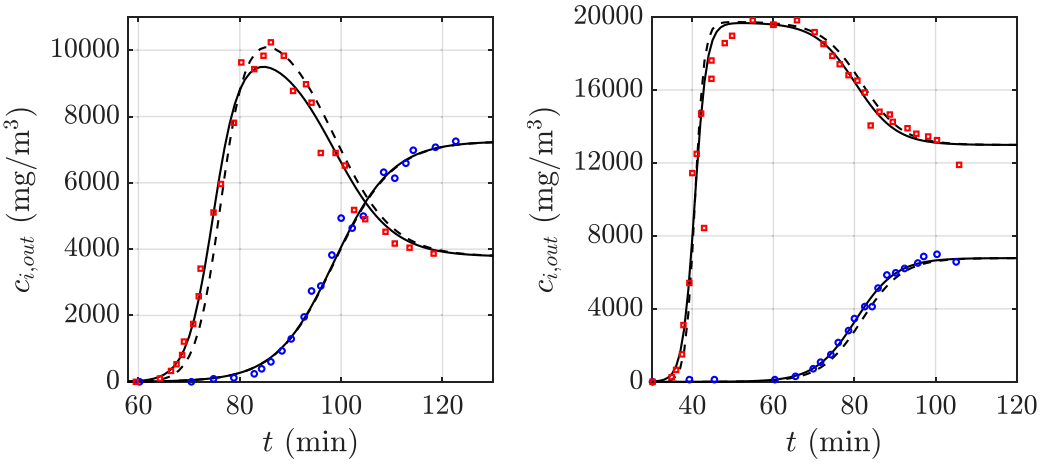

Fig. 13. Comparison between experimental and modelled breakthrough curves for heptane (blue) and cyclohexane (red) across datasets 3 (left panel) and 4 (right panel). Dashed lines represent predictions using equilibrium-derived parameters, while solid lines show results from direct optimisation of Eq. (7) to experimental data.

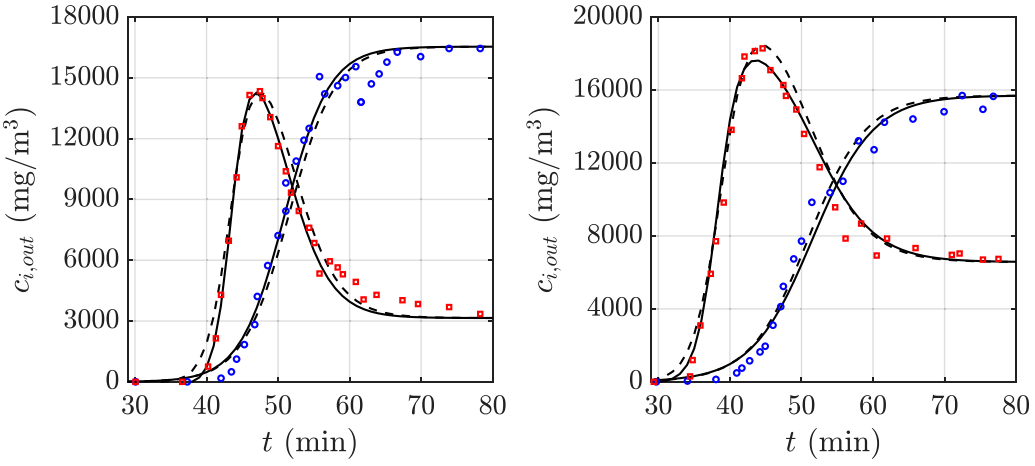

Fig. 14. Comparison between experimental and modelled breakthrough curves for heptane (blue) and cyclohexane (red) across datasets 5 (left panel) and 6 (right panel). Dashed lines represent predictions using equilibrium-derived parameters, while solid lines show results from direct optimisation of Eq. (7) to experimental data.

which shows the most pronounced deviation among all datasets. The unusually large deviation in the cyclohexane curve in dataset 7 is likely due to experimental error, as the irregular stepwise behaviour of the roll-up has a direct impact on the calculation of $q_{2,e}$.

Still, the relative deviations between predicted and fitted values of δ and $t_{i,h}$ remain below 15% and 19% for the D4–L2 and heptane–cyclohexane mixtures, respectively. The mean deviation of $k_{2,a}$ is below 17% for the D4–L2 system and 27% for the heptane–cyclohexane system. These results confirm the robustness of the approach.

6. Conclusions

This study shows that by linking dynamic adsorption experiments to their equilibrium state, we are capable of predicting key features of breakthrough curves using the two-component competitive model developed by Calvo-Schwarzwalder et al. [56] (CMCV model), thereby reinforcing the physical meaning of the parameters of the analytical model's parameters. By relying on previously fitted isotherm parameters, we move closer to using CMCV's analytical breakthrough model as a predictive tool, eliminating the need to fit each breakthrough curve individually and requiring only the fitting of a single kinetic constant.

Key findings include:

1. Single- and two-component Langmuir isotherms provided consistent and reliable estimates of equilibrium parameters, including maximum adsorption capacities and competitive constants.
2. Although desorption is neglected in the breakthrough model, its influence is preserved through the equilibrium behaviour captured in the isotherm data.
3. The competition parameter δ was predicted from isotherm parameters and concentration ratios, rather than fitted from breakthrough data. The predicted values matched well with experimental observations across all tests, validating its use as a fixed input.
4. Breakthrough front positions were accurately predicted using the isotherm-derived parameters and a single fitted value of the replacement rate $k_{1,r}$. The predictions outperformed the previous travelling-wave approximation, which systematically overestimated half-times due to its neglect of individual desorption rates.
5. The position of the dominant component's breakthrough curve and the full breakthrough curve of the weaker component were predicted with high accuracy using the isotherm-based model, achieving R^2 values above 0.97 in most cases and maintaining low relative error compared to the fully adjusted direct-fitting approach.

These results confirm that the analytical breakthrough model, when supported by equilibrium isotherm data, offers a practical and accurate framework for predicting multicomponent adsorption with minimal parameter adjustment. This approach reduces reliance on dynamic testing while maintaining strong predictive performance, making it especially useful for system design and early-stage screening of adsorbents.

For the cases where more than two contaminants are considered, it is important to emphasise that the mathematical model developed in this work can be extended in a natural way. However, it should also be stressed that the validity of the breakthrough model is restricted to systems in which the components exhibit sufficiently distinct half-times, since otherwise the underlying constant-pattern assumption would no longer hold. Future work will therefore explore the derivation of a more general solution applicable to systems where adsorbates with similar equilibrium capacities exhibit different dynamic behaviour, and the extension of this method to systems with more than two components, where the benefit of equilibrium-based predictions become even more pronounced.

Research data

The heptane-cyclohexane experimental data were taken from Vuong et al. [36]. The original experimental data has been made available online: https://github.com/marccalvoschwarzwalder/TwoComponentIsothermData

CRediT authorship contribution statement

A. Valverde: Writing – original draft, Validation, Software, Investigation, Formal analysis, Conceptualization. **T.G. Myers:** Writing – review & editing, Project administration, Funding acquisition, Conceptualization. **A. Cabrera-Codony:** Writing – original draft, Resources, Methodology, Data curation. **H.M. Thompson:** Writing – review & editing, Validation, Software. **G. Moncusí-Prieto:** Investigation, Data curation. **M. Calvo-Schwarzwalder:** Writing – original draft, Supervision, Investigation, Formal analysis, Conceptualization.

Declaration of competing interest

The authors declare that they have no known competing financial interests or personal relationships that could have appeared to influence the work reported in this paper.

Acknowledgements

This publication is part of the research projects Minerva (PID2023-146332OB-C21) and ShERLOcK (PID2020-112615RA-I00) financed by MCIN/AEI/ 10.13039/501100011033/, by "ERDF A way of making Europe" and by "European Union NextGenerationEU/PRTR". A. Cabrera-Codony acknowledges financial support from the Catalan government (2021-SGR-01352). M. Calvo-Schwarzwalder acknowledges financial support from the Catalan government (2021-SGR-00087). This work is supported by the Spanish State Research Agency, through the Severo Ochoa and Maria de Maeztu Program for Centres and Units of Excellence in R&D (CEX2020-001084-M). A. Valverde and M. Calvo-Schwarzwalder are Serra-Hunter fellows from the Serra-Hunter Programme of the Generalitat de Catalunya. T. G. Myers thanks CERCA Programme/Generalitat de Catalunya for institutional support. Open access funding was provided thanks to the CRUE-CSIC agreement with Elsevier. Funding from the MISSION-CCS (Material Science Innovation for Accelerated, Sustainable and Safe Implementation of Carbon Capture and Storage) Marie Sklodowska-Curie Actions Doctoral Network (MSCA-DN) program, grant number 101118369, and the UK government's Horizon Europe funding guarantee grant number EP/Y036980/1, is gratefully acknowledged.

Appendix A. Supplementary data

Supplementary material related to this article can be found online at https://doi.org/10.1016/j.jhazmat.2026.142572.

Data availability

The experimental data has been made available online: https://github.com/marccalvoschwarzwalder/TwoComponentIsothermData.

References

[1] Tran HN, Lima EC, Juang RS, Bollinger JC, Chao HP. Thermodynamic parameters of liquid–phase adsorption process calculated from different equilibrium constants related to adsorption isotherms: A comparison study. J Environ Chem Eng 2021;9:106674. http://dx.doi.org/10.1016/j.jece.2021.106674.

[2] Aguilera P, Gutiérrez Ortiz F. Prediction of fixed-bed breakthrough curves for H_2S adsorption from biogas: Importance of axial dispersion for design. Chem Eng J 2016;289:93–8. http://dx.doi.org/10.1016/j.cej.2015.12.075.

[3] Cabrera-Codony A, Ruiz B, Gil R, Popartan L, Santos-Clotas E, Martin M, Fuente E. From biocollagenic waste to efficient biogas purification: Applying circular economy in the leather industry. Environ Technol Innov 2021;21:101229. http://dx.doi.org/10.1016/j.eti.2020.101229.

[4] Yao C, Chen T. A new simplified method for estimating film mass transfer and surface diffusion coefficients from batch adsorption kinetic data. Chem Eng J 2015;265:93–9. http://dx.doi.org/10.1016/J.CEJ.2014.12.005.

[5] Wan Ngah WS, Teong LC, Toh RH, Hanafiah MAKM. Utilization of chitosan-zeolite composite in the removal of Cu(II) from aqueous solution: Adsorption, desorption and fixed bed column studies. Chem Eng J 2012;209:46–53. http://dx.doi.org/10.1016/j.cej.2012.07.116.

[6] Patiño Y, Diaz E, Ordóñez S. Pre-concentration of nalidixic acid through adsorption-desorption cycles: Adsorbent selection and modeling. Chem Eng J 2016;283:486–94. http://dx.doi.org/10.1016/j.cej.2015.07.084.

[7] Ruiz B, Cabrera-Codony A, Giron RP, Anfruns A, Martin MJ, Suarez-Ruiz I, Fuente E. From fly ashes of lignocellulose waste combustion to sustainable activated carbons for VOCs removal. Sustain Chem Pharm 2025;44:101943. http://dx.doi.org/10.1016/j.scp.2025.101943.

[8] Tovar-Gómez R, Moreno-Virgen MR, Dena-Aguilar JA, Hernández-Montoya V, Bonilla-Petriciolet A, Montes-Morán MA. Modeling of fixed-bed adsorption of fluoride on bone char using a hybrid neural network approach. Chem Eng J 2013;228:1098–109. http://dx.doi.org/10.1016/j.cej.2013.05.080.

[9] Garcia-Mateos FJ, Ruiz-Rosas R, Marques MD, Cotoruelo LM, Rodriguez-Mirasol J, Cordero T. Removal of paracetamol on biomass-derived activated carbon: Modeling the fixed bed breakthrough curves using batch adsorption experiments. Chem Eng J 2015;279:18–30. http://dx.doi.org/10.1016/j.cej.2015.04.144.

[10] Cheng H, Song H, Toan S, Wang B, Gasem KAM, Fan M, Cheng F. Experimental investigation of CO_2 adsorption and desorption on multi-type amines loaded HZSM-5 zeolites. Chem Eng J 2021;406:126882. http://dx.doi.org/10.1016/j.cej.2020.126882.

[11] López L, Dessi P, Cabrera-Codony A, Rocha-Melogno L, Kraakman N, Balaguer M, Puig S. Indoor CO_2 direct air capture and utilization: Key strategies towards carbon neutrality. Clean Eng Technol 2024;20:100746. http://dx.doi.org/10.1016/j.clet.2024.100746.

[12] Elfving J, Sainio T. Kinetic approach to modelling CO_2 adsorption from humid air using amine-functionalized resin: Equilibrium isotherms and column dynamics. Chem Eng Sci 2021;246:116885. http://dx.doi.org/10.1016/j.ces.2021.116885.

[13] Wang J, Xie D, Zhang Z, Yang Q, Xing H, Yang Y, Ren Q, Bao Z. Efficient adsorption separation of acetylene and ethylene via supported ionic liquid on metal-organic framework. AIChE J 2017;63(6):2165–75. http://dx.doi.org/10.1002/aic.15561.

[14] Wang H, Jahandar Lashaki M, Fayaz M, Hashisho Z, Philips JH, Anderson JE, Nichols M. Adsorption and desorption of mixtures of organic vapors on beaded activated carbon. Environ Sci Technol 2012;46(15):8341–50. http://dx.doi.org/10.1021/es3013062.

[15] Liu J, Li Y, Wang Y, Wang Y, Xu J, Liu X. Competitive adsorption of lead and cadmium on soil aggregate at micro-interfaces: Multi-surface modeling and spectroscopic studies. J Hazard Mater 2023;448:130915. http://dx.doi.org/10.1016/j.jhazmat.2023.130915.

[16] Tefera DT, Hashisho Z, Philips JH, Anderson JE, Nichols M. Modeling competitive adsorption of mixtures of volatile organic compounds in a fixed-bed of beaded activated carbon. Environ Sci Technol 2014;48(9):5108–17. http://dx.doi.org/10.1021/es404667f.

[17] Jagadeesh N, Sundaram B. Adsorption of pollutants from wastewater by biochar: A review. J Hazard Mater Adv 2023;9:100226. http://dx.doi.org/10.1016/j.hazadv.2022.100226.

[18] Meng Z, Huang S, Wu J, Lin Z. Competitive adsorption and immobilization of Cd, Ni, and Cu by biochar in unsaturated soils under single-, binary-, and ternary-metal systems. J Hazard Mater 2023;451:131106. http://dx.doi.org/10.1016/j.jhazmat.2023.131106.

[19] Jahandar Lashaki M, Kamravaei S, Hashisho Z, Phillips JH, Crompton D, Anderson JE, Nichols M. Adsorption and desorption of a mixture of volatile organic compounds: Impact of activated carbon porosity. Sep Purif Technol 2023;314:123530. http://dx.doi.org/10.1016/j.seppur.2023.123530.

[20] Çetin Güngör, Şakir Ece M. Competitive adsorption of VOCs (benzene, xylene and ethylbenzene) with Fe_3O_4@SiO_2-NH@BENZOPHENONE magnetic nanoadsorbents. Chem Eng J 2023;475:146034. http://dx.doi.org/10.1016/j.cej.2023.146034.

[21] Pour SE, Haghighat Mamaghani A, Hashisho Z, Crompton D, Arellano H, Anderson JE. Experimental and modeling study of volatile organic compounds adsorption over zeolitic monolith adsorbent. Chem Eng J 2024;246:148956. http://dx.doi.org/10.1016/j.cej.2024.148956.

[22] Singh M, Hakimabadi SG, Van Geel PJ, Carey GR, Pham ALT. Modified competitive langmuir model for prediction of multispecies PFAS competitive adsorption equilibria on colloidal activated carbon. Sep Purif Technol 2024;345:127368. http://dx.doi.org/10.1016/j.seppur.2024.127368.

[23] Butler J, Ockrent C. Studies in electrocapillarity. Part III: The surface tensions of solutions containing two surface-active solutes. J Phys Chem 1930;34:2841–59. http://dx.doi.org/10.1021/j150318a015.

[24] Jain JS, Snoeyink VL. Adsorption from bisolute systems on active carbon. J (Water Pollut Control Fed) 1973;45(12):2463–79, URL https://www.jstor.org/stable/25038061.

[25] Myers AL, Prausnitz JM. Thermodynamics of mixed-gas adsorption. AIChE J 1965;11(1):121–7. http://dx.doi.org/10.1002/aic.690110125.

[26] Crittenden JC, Luft P, Hand DW. Prediction of multicomponent adsorption equilibria in background mixtures of unknown composition. Water Res 1985;19(12):1537–48. http://dx.doi.org/10.1016/0043-1354(85)90399-9.

[27] Haider Jaffari Z, Jeong H, Shin J, Kwak J, Son C, Lee Y-G, Kim S, Chon K, Hwa Cho K. Machine-learning-based prediction and optimization of emerging contaminants' adsorption capacity on biochar materials. Chem Eng J 2023;466:143073. http://dx.doi.org/10.1016/j.cej.2023.143073.

[28] Bai S, Li J, Ding W, Chen S, Ya R. Removal of boron by a modified resin in fixed bed column: Breakthrough curve analysis using dynamic adsorption models and artificial neural network model. Chemosphere 2022;296:134021. http://dx.doi.org/10.1016/j.chemosphere.2022.134021.

[29] Cooney DO, Strusi FP. Analytical description of fixed-bed sorption of two Langmuir solutes under nonequilibrium conditions. Ind Eng Chem Fundam 1972;11(1):123–6. http://dx.doi.org/10.1021/i160041a018.

[30] Miura K, Kurahashi H, Inokuchi Y, Hashimoto K. A method for calculating breakthrough curves of bicomponent fixed-bed adsorption under constant pattern and linear driving force. J Chem Eng Jpn 1979;12(4):281–8. http://dx.doi.org/10.1252/jcej.12.281.

[31] Huang D, Saleem H, Guo B, Brusseau ML. The impact of multiple-component PFAS solutions on fluid-fluid interfacial adsorption and transport of PFOS in unsaturated porous media. Sci Total Environ 2022;806:150595. http://dx.doi.org/10.1016/j.scitotenv.2021.150595.

[32] Augelletti R, Conti M, Annesini MC. Pressure swing adsorption for biogas upgrading. A new process configuration for the separation of biomethane and carbon dioxide. J Clean Prod 2017;140:1390–8. http://dx.doi.org/10.1016/j.jclepro.2016.10.013.

[33] Guo S, Wang Z, Wu S, Cai Y, Zhang J, Lou C, Zhao W. Modification of the adsorption model for the mixture of odor compounds and VOCs on activated carbon: Insights from pore size distribution. Sep Purif Technol 2024;339:126669. http://dx.doi.org/10.1016/j.seppur.2024.126669.

[34] Luz AD, Guelli Ulson de Souza SMdA, da Luz C, Rezende RVdP, Ulson de Souza AA. Multicomponent adsorption and desorption of BTX compounds using coconut shell activated carbon: Experiments, mathematical modeling, and numerical simulation. Ind Eng Chem Res 2013;52(23):7896–911. http://dx.doi.org/10.1021/ie302849j.

[35] Fabian Ramos HS, Baliga C, Rajendran A, Nikrityuk PA. CFD-based model of adsorption columns: Validation. Chem Eng Sci 2024;285:119606. http://dx.doi.org/10.1016/j.ces.2023.119606.

[36] Vuong F, Chauveau R, Grevillot G, Marsteau S, Silvente E, Vallieres C. Predicting the lifetime of organic vapor cartridges exposed to volatile organic compound mixtures using a partial differential equations model. J Occup Environ Hyg 2016;13(9):675–89. http://dx.doi.org/10.1080/15459624.2016.1166368.

[37] Suzaki PYR, Triques CC, Munaro MT, Steffen V, Kleinübing SJ, Klen MRF, Bergamasco R, de Matos Jorge LM. Phenomenological modeling and simulation of competitive biosorption of ternary heavy metal systems in a fixed bed column. Chem Eng Res Des 2023;196:701–10. http://dx.doi.org/10.1016/j.cherd.2023.07.009.

[38] Durán I, Rubiera F, Pevida C. Modeling a biogas upgrading PSA unit with a sustainable activated carbon derived from pine sawdust. Sensitivity analysis on the adsorption of CO2 and CH4 mixtures. Chem Eng J 2022;428:132564. http://dx.doi.org/10.1016/j.cej.2021.132564.

[39] Streb A, Mazzotti M. Adsorption for efficient low carbon hydrogen production: part 1—adsorption equilibrium and breakthrough studies for H2/CO2/CH4 on zeolite 13x. Adsorption 2021;27(4):541–58. http://dx.doi.org/10.1007/s10450-021-00306-y.

[40] Canevesi RLS, Andreassen KA, da Silva EA, Borba CE, Grande CA. Pressure swing adsorption for biogas upgrading with carbon molecular sieve. Ind Eng Chem Res 2018;57(23):8057–67. http://dx.doi.org/10.1021/acs.iecr.8b00996.

[41] Grande CA, Rodrigues AE. Biogas to fuel by vacuum pressure swing adsorption I. Behavior of equilibrium and kinetic-based adsorbents. Ind Eng Chem Res 2007;46(13):4595–605. http://dx.doi.org/10.1021/ie061341+.

[42] Lopes FV, Grande CA, Rodrigues AE. Activated carbon for hydrogen purification by pressure swing adsorption: Multicomponent breakthrough curves and PSA performance. Chem Eng Sci 2011;66(3):303–17. http://dx.doi.org/10.1016/j.ces.2010.10.034.

[43] Song F, Islam M. A new mathematical model and experimental validation of multicomponent adsorption. In: SPE improved oil recovery conference. vol. SPE/DOE Improved Oil Recovery Symposium, 1994, p. SPE–27838–MS. http://dx.doi.org/10.2118/27838-MS.

[44] Sharma S, Balestra SRG, Baur R, Agarwal U, Zuidema E, Rigutto MS, Calero S, Vlugt TJH, Dubbeldam D. RUPTURA: simulation code for breakthrough, ideal adsorption solution theory computations, and fitting of isotherm models. Mol Simul 2023;49(9):893–953. http://dx.doi.org/10.1080/08927022.2023.2202757.

[45] Berg F, Gohlke K, Pasel C, Luckas M, Eckardt T, Bathen D. Single and binary mixture adsorption behaviors of C6–C8 hydrocarbons on silica–alumina gel. Ind Eng Chem Res 2018;57(48):16451–63. http://dx.doi.org/10.1021/acs.iecr.8b04498.

[46] Gironi F, Piemonte V. VOCs removal from dilute vapour streams by adsorption onto activated carbon. Chem Eng J 2011;172(2):671–7. http://dx.doi.org/10.1016/j.cej.2011.06.034.

[47] Heymans N, Vaesen S, De Weireld G. A complete procedure for acidic gas separation by adsorption on MIL-53 (Al). Microporous Mesoporous Mater 2012;154:93–9. http://dx.doi.org/10.1016/j.micromeso.2011.10.020, Special Issue: Characterisation of Porous Solids IX.

[48] Chouikhi N, Brandani F, Pullumbi P, Perre P, Puel F. Biomethane production by adsorption technology: new cycle development, adsorbent selection and process optimization. Adsorption 2020;26(8):1275–89. http://dx.doi.org/10.1007/s10450-020-00250-3.
[49] Mazzotti M, Rajendran A. Equilibrium theory–based analysis of nonlinear waves in separation processes. Annu Rev Chem Biomol Eng 2013;4(Volume 4, 2013):119–41. http://dx.doi.org/10.1146/annurev-chembioeng-061312-103318.
[50] Zarei S, Harriehausen I, Lee JW, Seidel-Morgenstern A. Equilibrium loadings and adsorption isotherm model parameters estimated from multi-component breakthrough curves. Adsorption 2024;30(8):2295–312. http://dx.doi.org/10.1007/s10450-024-00549-5.
[51] Nagel G, Kluge G, Flock W. Modelling of non-isothermal multi-component adsorption in adiabatic fixed beds-I. The numerical solution of the parallel diffusion model. Chem Eng Sci 1987;42(1):143–53. http://dx.doi.org/10.1016/0009-2509(87)80217-8.
[52] Rhee H-K, Amundson NR. An analysis of an adiabatic adsorption column: Part 1. Theoretical development. Chem Eng J 1970;1(3):241–54. http://dx.doi.org/10.1016/0300-9467(70)80007-7.
[53] Rhee H-K, Amundson NR. On the theory of multicomponent chromatography. Philos Trans R Soc Lond Ser A, Math Phys Sci 1970;267(1182):419–55. http://dx.doi.org/10.1098/rsta.1970.0050.
[54] Liapis A, Rippin D. The simulation of binary adsorption in activated carbon columns using estimates of diffusional resistance within the carbon particles derived from batc. Chem Eng Sci 1978;33(5):593–600. http://dx.doi.org/10.1016/0009-2509(78)80021-9.
[55] Liapis AI, Rippin DWT. The simulation of binary adsorption in continuous countercurrent operation and a comparison with other operating modes. AIChE J 1979;25(3):455–60. http://dx.doi.org/10.1002/aic.690250310.
[56] Calvo-Schwarzwalder M, Myers TG, Cabrera-Codony A, Valverde A. An analytical breakthrough model for adsorption systems with two competing contaminant species. Int J Heat Mass Transf 2025;245:127004. http://dx.doi.org/10.1016/j.ijheatmasstransfer.2025.127004.
[57] Liu Z, Sun Z, Zhang L, Xu L, Lu X, Cui Q, Wang H. Template-free synthesis of hierarchical nanocrystal UiO-66 and its adsorption thermodynamics for n-heptane and methyl cyclohexane. Cryst Eng Comm 2021;23:4549–59. http://dx.doi.org/10.1039/D1CE00438G.
[58] Dufresne M, Salameh T, Leonardis T, Gille G, Armengaud A, Sauvage S. Volatile organic compound sources and impacts in an urban Mediterranean area (Marseille, France). Atmospheric Chem Phys 2025;25(11):5977–99. http://dx.doi.org/10.5194/acp-25-5977-2025.
[59] Rajabi H, Hadi Mosleh M, Mandal P, Lea-Langton A, Sedighi M. Emissions of volatile organic compounds from crude oil processing – Global emission inventory and environmental release. Sci Total Environ 2020;727:138654. http://dx.doi.org/10.1016/j.scitotenv.2020.138654.
[60] Cabrera-Codony A, Santos-Clotas E, Ania C, Martin M. Competitive siloxane adsorption in multicomponent gas streams for biogas upgrading. Chem Eng J 2018;344:565–73. http://dx.doi.org/10.1016/j.cej.2018.03.131.
[61] Santos-Clotas E, Cabrera-Codony A, Martin MJ. Coupling adsorption with biotechnologies for siloxane abatement from biogas. Renew Energy 2019;153:314–23. http://dx.doi.org/10.1016/j.renene.2020.02.026.
[62] Myers TG, Cabrera-Codony A, Valverde A. On the development of a consistent mathematical model for adsorption in a packed column (and why standard models fail). Int J Heat Mass Transfer 2023;202:123660. http://dx.doi.org/10.1016/j.ijheatmasstransfer.2022.123660.
[63] Markham EC, Benton AF. The adsorption of gas mixtures by silica. J Am Chem Soc 1931;53(2):497–507. http://dx.doi.org/10.1021/ja01353a013.
[64] Langmuir I. The adsorption of gases on plane surfaces of glass, mica and platinum. J Am Chem Soc 1918;40(9):1361–403. http://dx.doi.org/10.1021/ja02242a004.
[65] Wilkins NS, Rajendran A. Measurement of competitive CO2 and N2 adsorption on zeolite 13X for post-combustion CO2 capture. Adsorption 2019;25(2):115–33. http://dx.doi.org/10.1007/s10450-018-00004-2.
[66] Wilkins NS, Rajendran A, Farooq S. Dynamic column breakthrough experiments for measurement of adsorption equilibrium and kinetics. Adsorption 2021;27(3):397–422. http://dx.doi.org/10.1007/s10450-020-00269-6.
[67] Van Assche TR, Wittevrongel GR, Lozano Betancur V, Muslumzada L, Denayer JF. Graphical method to obtain multicomponent adsorption equilibria from intermediate breakthrough curve plateaus. Chem Eng Sci 2023;282:119323. http://dx.doi.org/10.1016/j.ces.2023.119323.
[68] Marler R, Arora J. Survey of multi-objective optimization methods for engineering. Struct Multidiscip Optim 2004;26:369–95. http://dx.doi.org/10.1007/s00158-003-0368-6.
[69] Zelany M. A concept of compromise solutions and the method of the displaced ideal. Comput Oper Res 1974;1(3):479–96. http://dx.doi.org/10.1016/0305-0548(74)90064-1.
[70] Giannikopoulos I, Skouteris A, Allen D, Baldea M, Stadtherr M. Multi-objective optimization of production cost and carbon loss in the U.S. petrochemicals industry. In: Yamashita Y, Kano M, editors. 14th international symposium on process systems engineering. Computer aided chemical engineering, vol. 49, Elsevier; 2022, p. 547–52. http://dx.doi.org/10.1016/B978-0-323-85159-6.50091-9.
[71] Grodzevich O, Romanko O. Normalization and other topics in multi-objective optimization. In: Proceedings of the fields-MITACS industrial problems workshop. 2006, p. 89–101.
[72] Wang G, Dou B, Zhang Z, Wang J, Liu H, Hao Z. Adsorption of benzene, cyclohexane and hexane on ordered mesoporous carbon. J Environ Sci 2015;30:65–73. http://dx.doi.org/10.1016/j.jes.2014.10.015.
[73] Amaraibi RJ, Reynolds B, Joseph B, Kuhn JN. Experimental, economic, and life cycle carbon footprint assessment of low-cost adsorbents for siloxane removal from landfill gas. Environ Prog Sustain Energy 2025;44(1):e14534. http://dx.doi.org/10.1002/ep.14534.
[74] Aguareles M, Barrabés E, Myers TG, Valverde A. Mathematical analysis of a Sips-based model for column adsorption. Phys D: Nonlinear Phenom 2023;448:133690. http://dx.doi.org/10.1016/j.physd.2023.133690.
[75] Sips R. On the structure of a catalyst surface. J Chem Phys 1948;16(5):490–5. http://dx.doi.org/10.1063/1.1746922.
[76] Rudziński W, Nieszporek K, Moon H, Rhee H-K. On the theoretical origin and applicability of the potential theory approach to predict mixed-gas adsorption on solid surfaces from single-gas adsorption isotherms. Chem Eng Sci 1995;50(16):2641–60. http://dx.doi.org/10.1016/0009-2509(95)00100-J.